THE ASTROPHYSICAL JOURNAL, 230:49–67, 1979 May 15

A HIGH-RESOLUTION STUDY OF THE ABSORPTION SPECTRA OF THE QSOs Q0002−422 AND Q0453−423

WALLACE L. W. SARGENT AND PETER J YOUNG
Hale Observatories, California Institute of Technology, Carnegie Institution of Washington
A. BOKSENBERG
Department of Physics and Astronomy, University College London
AND
R. F. CARSWELL AND J. A. J. WHELAN
Institute of Astronomy, Cambridge University
Received 1978 August 4; accepted 1978 November 9

ABSTRACT

High-resolution (0.8 Å FWHM) spectroscopic observations over the wavelength range 3800 Å–5400 Å are presented for the two bright southern QSOs, Q0002−422 (z_{em} = 2.763) and Q0453−423 (z_{em} = 2.656). For these two objects we list 80 and 77 absorption lines, respectively, and identify five absorption-line systems in each object, ranging from z_{abs} = 0.7261 to z_{abs} = 2.4641. All lines longward of Lα emission are successfully identified, but only 18% of those shortward of Lα have yielded to our investigation.

A study of the metal-rich absorption systems identified in the two objects here and also in PKS 2126−158 strongly support the notion that the lines originate in galactic halos. The density of systems requires halos of radius ∼30 kpc. The systems at high redshift (z_{abs} ∼ 2.5) probably arise from photoionized gas (possibly by the integrated QSO light) and have $N(\mathrm{H}) \sim 10^{20}\ \mathrm{cm}^{-3}$, $n(\mathrm{H}) \sim 0.3\ \mathrm{cm}^{-3}$, diameter $D \sim 3 \times 10^{20}$ cm, $T_e = 10^4$ K, and $M \sim 10^3\ M_\odot$. Roughly 10^6 objects per galactic halo (of total mass $\sim 10^9\ M_\odot$) would be required, so that the clouds do not require a cosmologically significant density, with $\Omega_{cloud} = 10^{-3}$.

Subject headings: galaxies: structure — line identifications — quasars

I. INTRODUCTION

We continue our high-resolution studies of the absorption features in high-redshift QSOs with the pair Q0002−422 (z_{em} = 2.763) and Q0453−423 (z_{em} = 2.656) selected from the sample of bright, high-redshift QSOs discovered by Smith (1976). The QSOs were found on Cerro Tololo objective prism plates (Smith 1975). They have been studied at low (16 Å) resolution by Osmer and Smith (1976) and at intermediate (5 Å) resolution by Carswell, Smith, and Whelan (1977, hereafter CSW) and by Whelan, Carswell, and Smith (1977, hereafter WCS). We present new observations at 0.8 Å resolution (FWHM) with uniform signal-to-noise ratio over a spectral range of 1600 Å in the blue. This yields data both longward and shortward of the Lα emission line, and allows study of both the few strong, metal-rich absorption-line systems and the weaker systems containing only Lα absorption, which appear to predominate among the absorption lines shortward of the Lα emission line in high-redshift QSOs (Lynds 1971).

The purpose of this paper is to present the absorption-line lists for the two QSOs together with identifications in the strong absorption-line systems. The high resolution and accurate wavelengths reduce significantly the possibility of spurious absorption systems; the noise due to such systems varies as the cube of the acceptance window (Aaronson, McKee, and Weisheit 1975). We also discuss the data for PKS 2126−158 (z_{em} = 3.280), which were studied by Young *et al.* (1979, hereafter Paper I), in order to obtain the physical conditions in the gas producing the metal-line absorption systems.

In § II, we detail the observational procedure and compilation of the emission- and absorption-line lists. In § III, we identify the absorption-line systems, and in § IV, we discuss the origin of the absorption systems. The conclusions are summarized in § V.

II. OBSERVATIONS AND INITIAL REDUCTIONS

a) Observations

Observations of Q0002−422 and Q0453−423 were obtained in 1976 November employing the University College London Image Photon Counting System (IPCS) mounted on the RGO spectrograph at the Cassegrain focus of the Anglo-Australian 3.9 m telescope. A journal of observations is given in Table 1. A 1200 lines per mm

TABLE 1

OBSERVATIONS OF Q0002−422 AND Q0453−423

Date	Exp. (s)	λ-Range (Å)	Pixel Format	Pixel Size (Å)	Resol. FWHM (Å)	Rebinned Data λ-Range (Å)	Rebinned Data No. of Pixels	Rebinned Data Mean Count Level*
			Q0002−422					
1976 Nov.....	6000	4070–4870	1750 × 10	0.46	0.82	4072.74–4861.44	2060	60
1976 Nov.....	6000	4640–5430	1750 × 10	0.45	0.71	4645.00–5422.02	1800	90
1976 Nov.....	7200	3750–4570	1750 × 10	0.47	0.84	3759.93–4569.78	2270	70
			Q0453−423					
1976 Nov.....	8800	4070–4870	1750 × 10	0.46	0.82	4072.47–4861.12	2060	90
1976 Nov.....	4000	4640–5430	1750 × 10	0.45	0.71	4648.68–5412.34	1800	70
1976 Nov.....	8400	3810–4620	1750 × 10	0.47	0.95	3815.00–4616.83	2220	60

* In continuum, away from emission lines.

grating blazed in first order at λ4600 was used, together with an f/1.67 camera of focal length 25 cm. The resulting dispersion was 25 Å mm^{-1}. A slit width of 1″.5 (220 μm) was chosen so as to project onto two resolution elements in the detector, each element being 0.46 Å wide. Simultaneous sky subtraction was achieved by using the IPCS in a two-dimensional mode. The wavelength scale was established by fitting polynomials to Cu-A arcs which were exposed frequently during the course of the observations. The unblended lines chosen left residuals of <0.1 Å after determination of terms up to fifth order. The data were divided by a flat field and were sky subtracted in the manner described by Sargent *et al.* (1978) before being rebinned on a logarithmic wavelength scale with $\Delta\lambda/\lambda = 8.59315 \times 10^{-5}$ (25.78 km s^{-1} per channel). All wavelengths are given as vacuum-reduced, heliocentric values.

Each QSO was observed in three wavelength regions with overlapping segments. These spectra are displayed in Figures 1 and 2. The segments were not added in order to ensure that a relatively uniform signal-to-noise ratio existed over the whole spectrum, thus aiding the homogeneity of line selection procedures, and allowing independent checks on the accuracy of wavelength and equivalent width.

b) Emission Lines

In Table 2, we give the observed wavelengths and equivalent widths of the emission lines observed in both QSOs. The equivalent widths were determined by planimetering small scale plots of the high-resolution data. The quoted wavelengths are for the "center of luminosity" of each line, since this is a quantity that may be reliably

TABLE 2

EMISSION LINES IN Q0002−422, Q0453−423

Ion	λ_{rest} (Å)	λ_{obs} (Å)	z_{em}	W_{obs} (Å)	W_{rest} (Å)
		Q0002−422			
O IV.....	1034	3886 ± 2	2.758 ± 0.002	30 ± 4	8.0 ± 1.1
S III.....	1078	4051 ± 3	2.758 ± 0.003	19 ± 3	5.1 ± 0.8
H I.....	1215	4575 ± 3	2.763 ± 0.002	400 ± 50	106 ± 13
N V*.....	1240	...	...	83 ± 25	22 ± 7
O I.....	1304	4917 ± 4	2.768 ± 0.003	19 ± 5	5.1 ± 1.3
Si IV.....	1397	5265 ± 4	2.768 ± 0.003	21 ± 5	5.6 ± 1.3
$\langle z_{em} \rangle$.....			2.763 ± 0.005		
		Q0453−423			
H I.....	1215	4445 ± 3	2.656 ± 0.002	217 ± 30	59 ± 11
N V.....	1240	4529 ± 4	2.652 ± 0.003	22 ± 5	6.0 ± 1.9
O I.....	1305	4775 ± 5	2.659 ± 0.004	16 ± 4	4.4 ± 1.1
Si IV.....	1397	5107 ± 4	2.656 ± 0.003	23 ± 5	6.3 ± 1.9
$\langle z_{em} \rangle$.....			2.656 ± 0.003		

* Wavelength determination not possible owing to blending with Lα emission.

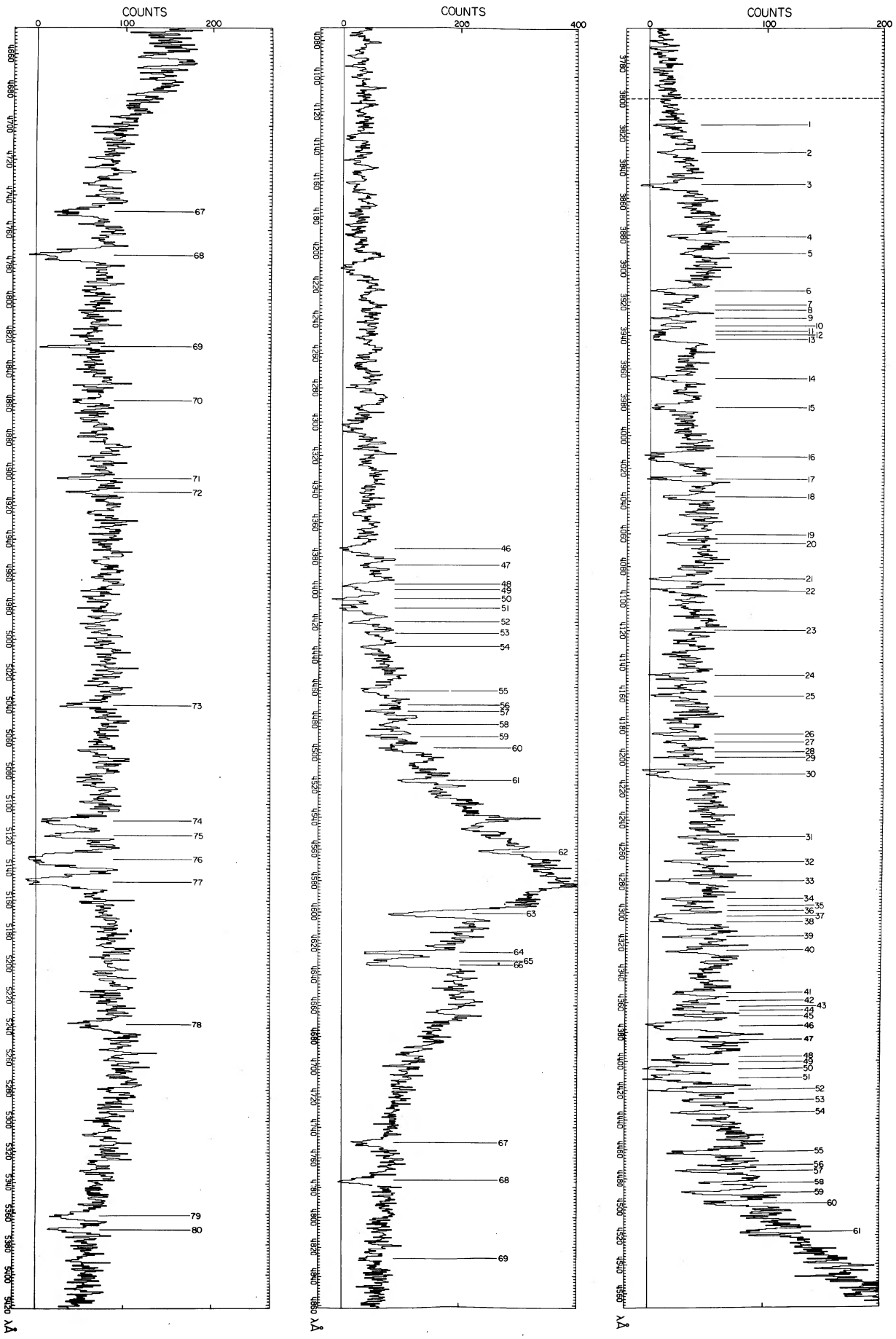

Fig. 1.—Spectrum of Q0002−422, showing three overlapping independent observations covering the range 3760 Å–5422 Å. Each bin is 25.78 km s^{-1}. The zero intensity level in each observation is indicated by a horizontal solid line. The vertical dashed line at 3800 Å shows the lower limit of usable data. The 80 absorption lines listed in Table 3 are marked and labeled.

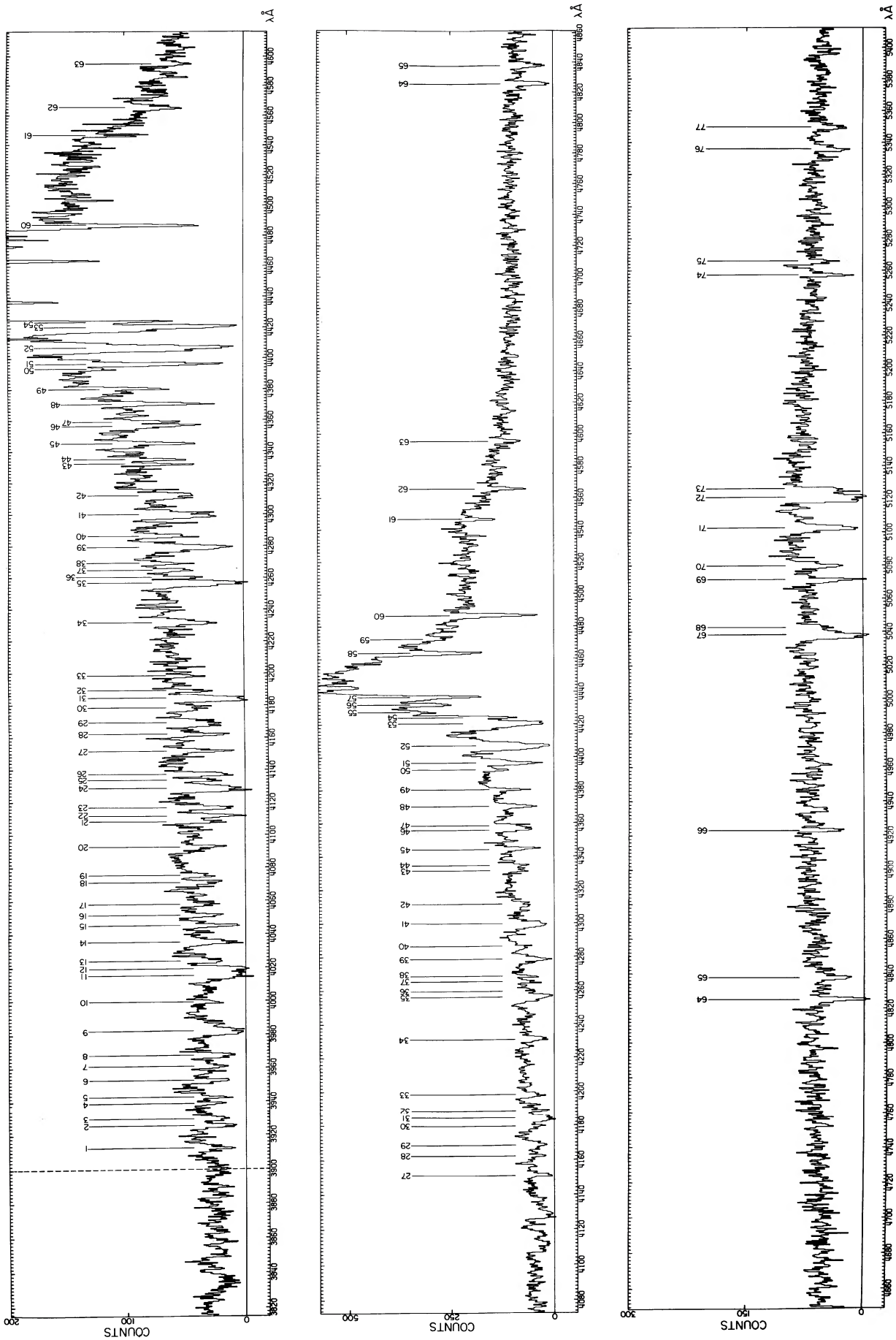

FIG. 2.—Spectrum of Q0453−423, showing three overlapping independent observations covering the range 3815 Å–5412 Å. Each bin is 25.78 km s^{-1}. The zero intensity level in each observation is indicated by a horizontal solid line. The vertical dashed line at 3900 Å shows the lower limit of usable data. The 77 absorption lines listed in Table 4 are marked and labeled.

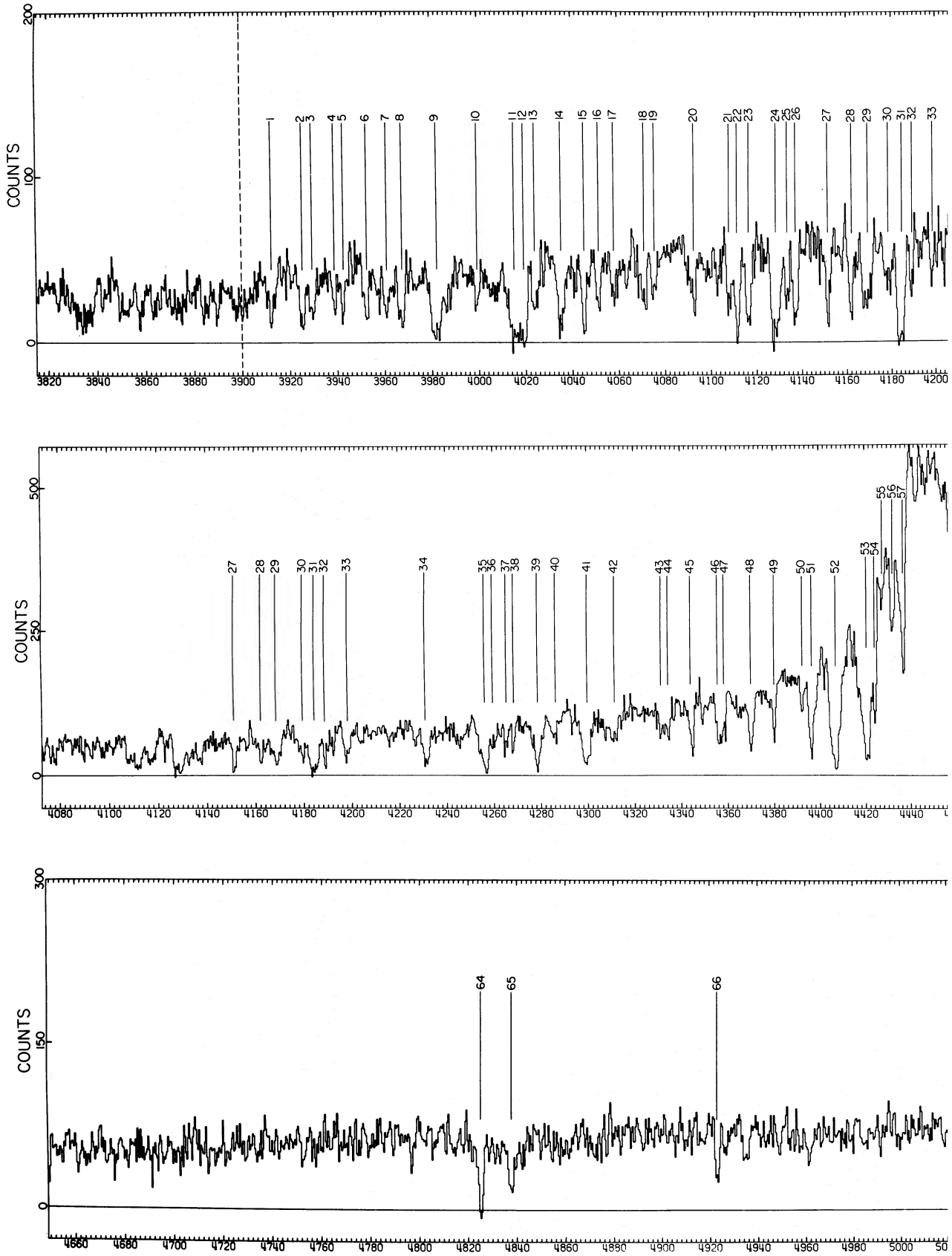

FIG. 2.—Spectrum of Q0453−423, showing three overlapping independent observations covering the range 3815 Å–5412 cal dashed line at 3900 Å shows the lower limit of usable data. The 77 absorption lines listed in Table 4 are marked and lat

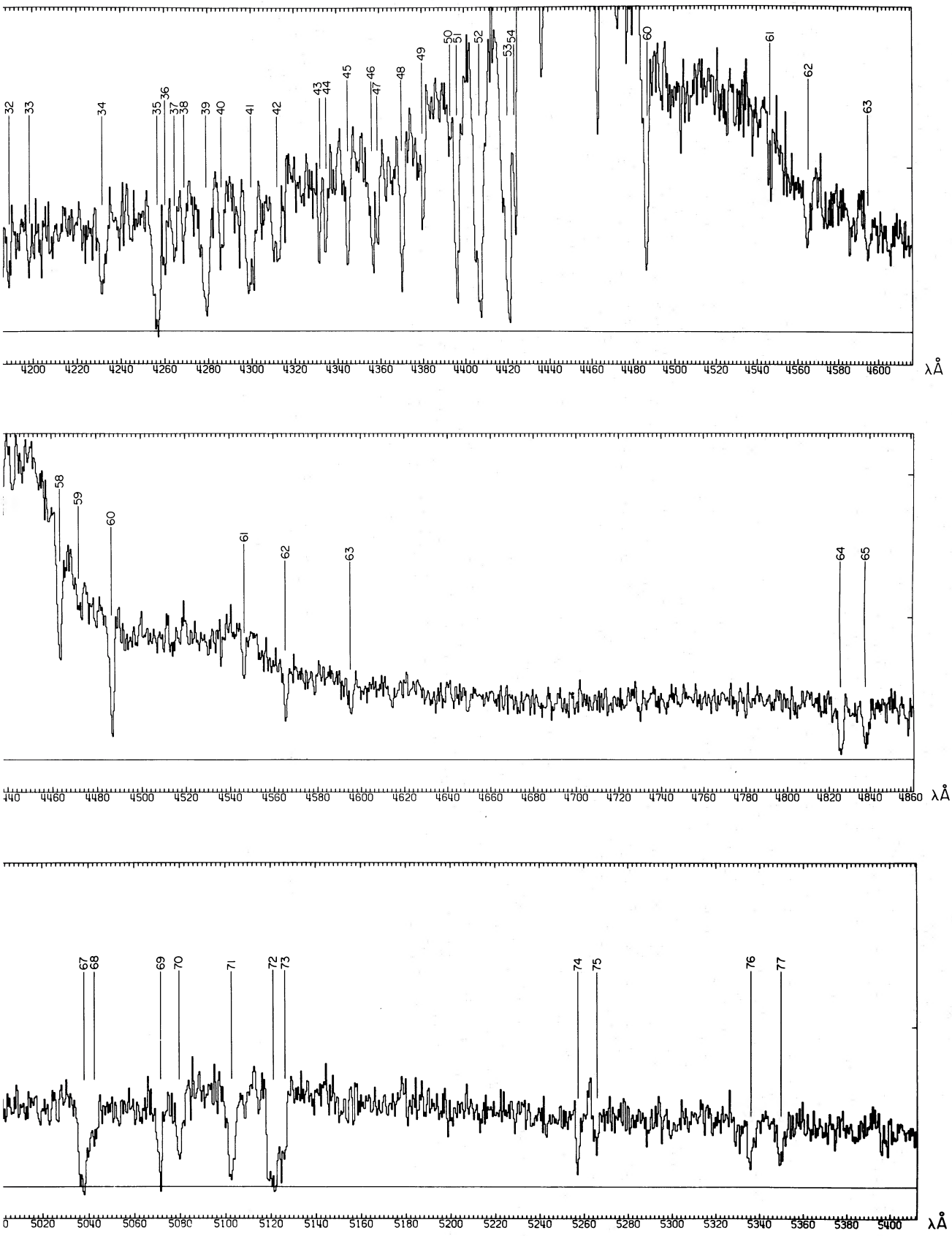

·5412 Å. Each bin is 25.78 km s^{-1}. The zero intensity level in each observation is indicated by a horizontal solid line. The verti-
nd labeled.

TABLE 3

Q0002−422: Absorption-Line List

n	λ(Å)	σ(λ)Å	W(Å)	σ(W)Å	N_c	Identification	z_{abs}	Comments
1	3815.9	0.2	1.2	0.1	23			
2	3832.2	0.5	1.9	0.2	33			
3	3851.8	0.3	3.6	0.4	38	H I(1215)	2.1685	
4	3881.7	0.2	1.9	0.2	48			
5	3891.3	0.3	1.3	0.1	49			
6	3914.2	0.3	2.9	0.3	39			
7	3922.1	0.4	1.3	0.2	38			
8	3924.8	0.4	1.3	0.2	38			
9	3930.2	0.2	2.3	0.2	37	Si II(1190)	2.3015	
10	3934.4	0.3	1.8	0.2	37			
11	3937.7	0.5	1.9	0.4	36			C1
12	3940.3	0.6	2.4	0.5	36	Si II(1193)	2.3021	C1
13	3942.3	0.5	2.4	0.5	36			C1
14	3966.3	0.3	2.5	0.3	31			
15	3983.5	0.2	3.1	0.3	31	Si III(1206)	2.3017	
16	4014.0	0.3	5.9	0.6	40	H I(1215)	2.3019	
17	4027.2	0.2	2.3	0.2	44			
18	4038.4	0.2	2.1	0.2	44			
19	4061.0	0.2	1.7	0.2	45			
20	4066.8	0.2	0.8	0.1	45			
21	4088.2	0.2	2.4	0.2	44			
22	4095.2	0.2	2.4	0.2	44			
23	4120.6	0.3	0.8	0.1	43			
24	4148.8	0.3	2.0	0.2	43,38			
25	4161.9	0.3	2.1	0.3	43,39	Si II(1260)	2.3020	
26	4186.1	0.2	1.7	0.2	45,41			
27	4191.1	0.3	1.4	0.1	46			
28	4197.4	0.2	1.0	0.1	46			
29	4200.5	0.3	1.2	0.1	47			
30	4211.3	0.4	6.2	0.6	48,51	H I(1215)	2.4642	
31	4251.8	0.2	1.0	0.1	53,52			
32	4268.0	0.2	1.5	0.1	57			
33	4280.3	0.3	2.1	0.2	57,58			
34	4292.2	0.2	1.7	0.2	58			
35	4295.8	0.3	1.5	0.1	58			
36	4299.2	0.3	0.9	0.1	58	O I(1302)	2.3016	
37	4303.1	0.5	2.8	0.5	59,60			C2
38	4306.6	0.5	2.7	0.5	59,60	Fe II(2344) Si II(1304)	0.8371 2.3017	C2
39	4317.1	0.2	0.9	0.1	60,58			
40	4326.6	0.4	1.3	0.1	61,56			
41	4354.8	0.2	1.9	0.2	63,49			
42	4359.7	0.3	1.3	0.1	63	Fe II(2374)	0.8367	
43	4363.0	0.3	1.1	0.1	63,51			
44	4365.4	0.3	1.3	0.1	63,51			
45	4369.7	0.2	1.1	0.1	63,52			
46	4376.4	0.3	5.1	0.5	63,56	Fe II(2382)	0.8367	
47	4386.1	0.2	1.5	0.2	63,64			
48	4397.7	0.6	2.2	0.4	63,62			C3
49	4400.8	0.6	1.9	0.4	63,62			C3
50	4406.1	0.2	3.4	0.4	63,62	C II(1334)	2.3016	
51	4412.1	0.3	4.7	0.4	63,64			
52	4420.3	0.2	2.4	0.2	63,71			
53	4427.6	0.2	1.1	0.1	63,73			
54	4435.9	0.2	1.3	0.1	64,75			
55	4462.9	0.2	2.3	0.2	78,86			
56	4471.8	0.2	0.5	0.1	82,87			
57	4475.6	0.2	1.1	0.1	84,88			

TABLE 3—*Continued*

n	λ(Å)	σ(λ)Å	W(Å)	σ(W)Å	N_c	Identification	z_{abs}	Comments
58	4483.9	0.4	1.1	0.1	90,96			
59	4491.0	0.3	1.7	0.2	95,105			
60	4498.4	0.3	1.7	0.2	101,119			
61	4518.0	0.2	0.9	0.1	118,162			
62	4562.7	0.2	0.5	0.1	290	Si II(1526)	1.9886	
63	4602.2	0.2	3.0	0.3	254	Si IV(1393)	2.3020	
64	4626.9	0.3	2.2	0.3	190	C IV(1548)	1.9886	C4
65	4632.0	0.5	2.5	0.5	190	Si IV(1402)	2.3020	C4
66	4634.6	0.5	1.9	0.5	190	C IV(1550)	1.9886	C4
67	4750.9	0.3	3.1	0.3	82,87	Fe II(2586)	0.8367	
68	4775.8	0.3	5.4	0.5	78,82	Fe II(2600)	0.8367	
69	4828.5	0.2	1.2	0.2	61,67	Si IV(1393)	2.4644	
70	4859.8	0.3	0.8	0.1	69	Si IV(1402)	2.4644	
71	4905.0	0.2	1.1	0.1	80	C IV(1548)	2.1662	
72	4913.2	0.2	0.9	0.2	80	C IV(1550)	2.1682	
73	5040.9	0.3	1.6	0.2	84	Si II(1526)	2.3018	
74	5111.9	0.2	3.8	0.4	84	C IV(1548)	2.3018	
75	5120.4	0.2	2.8	0.2	84	C IV(1550)	2.3018	
76	5135.4	0.3	8.6	0.7	84	Mg II(2796)	0.8365	
77	5149.0	0.3	7.4	0.6	84	Mg II(2803)	0.8366	
78	5239.6	0.3	2.5	0.2	94	Mg I(2852)	0.8365	
79	5362.6	0.2	2.5	0.2	66	C IV(1548)	2.4637	
80	5371.5	0.2	1.9	0.2	64	C IV(1550)	2.4637	

NOTES.—(1) Wavelength region analyzed: 3800 Å–5420 Å. (2) All wavelengths heliocentric, vacuum values. (3) N_c = number of counts in continuum near line. Two values given where line measured on two spectra. (4) Lines which are members of a confused complex (*J*) are denoted CJ.

determined. Our results are in good agreement with the values found by Osmer and Smith (1976), by CSW, and by WCS for those parameters determined both by them and by us.

c) Absorption Lines

The statistical considerations and the methods of measuring wavelengths and equivalent widths of absorption lines which were detailed in Paper I were also applied to Q0002−422 and Q0453−423. In particular, we required that a line be of minimum strength 4 σ. This resulted in the 80 lines for Q0002−422 listed in Table 3, and the 77 lines for Q0453−423 shown in Table 4. The quoted error estimates were calculated as in Paper I. For Q0002−422, we confirmed all the accessible lines in WCS, except for one at λ4649. However, there is a discrepancy of 4 Å between our wavelength scale and that of WCS. The scale used in the present work has been carefully checked and is accurate to 0.1 Å. For Q0453−423, we confirmed all the accessible lines in CSW, except for their line at λ4961.3, where our data show a feature which failed to meet our criteria for acceptance as a line.

III. ABSORPTION LINE SYSTEMS

a) Identification of Systems

The methods described in Paper I were applied in a uniform manner to all the data. The resulting absorption redshift systems for the two QSOs are given in Tables 5 and 6.

In Paper I, we defined four types of redshift systems—denoted by S_1, S_2, W_1, and W_2, respectively—which satisfy well-defined criteria for line strengths and redshift windows; this will eventually enable a uniform statistical analysis to be made of the number of redshift systems in different QSOs. We briefly summarize these definitions as follows:

1. S_1 systems are based on 12 lines: Lα λ1215, C II λ1334, C IV λλ1548, 1550, Si II λλ1190, 1193, 1260, 1304, 1526, Si III λ1206, and Si IV λλ1393, 1402. We demand that ≥8 lines be accessible in the wavelength region observed, and that ≥7 lines be visible with $W_{rest} \geq 0.25$ Å.

2. S_2 systems are based on eight lines: Mg I λ2852, Mg II λλ2796, 2803, and Fe II λλ2344, 2374, 2382, 2586, 2600. We demand that ≥5 lines be accessible, and that ≥4 lines be visible with $W_{rest} \geq 0.5$ Å.

These "strong" S_1 and S_2 systems are defined so that they may be discovered even when all the lines are shortward of the Lα emission line. This is not so for the "weak" systems W_1 and W_2, which we now define as follows:

3. W_1 systems must have the C IV λλ1548, 1550 doublet visible longward of Lα emission, both members having $W_{rest} > 0.25$ Å; also, C IV λ1548 must be stronger than C IV λ1550. In addition, ≥1 other lines must be visible anywhere in the spectrum.

TABLE 4

Q0453−423: ABSORPTION-LINE LIST

n	λ(Å)	σ(λ)Å	W(Å)	σ(W)Å	N_c	Identification	z_{abs}	Comments
1	3913.7	0.2	2.4	0.2	45			
2	3926.7	0.2	2.3	0.2	47			
3	3930.8	0.2	1.9	0.2	47			
4	3940.0	0.2	1.1	0.2	48			
5	3943.8	0.2	1.1	0.2	48			
6	3953.4	0.2	1.6	0.2	48	Si III(1206)	2.2767	
7	3962.1	0.2	1.6	0.2	47			
8	3968.4	0.2	2.2	0.2	46			
9	3983.1	0.3	4.2	0.4	43	H I(1215)	2.2764	
10	4000.5	0.3	1.0	0.2	44			
11	4016.4	0.6	4.0	0.6	47			C1
12	4020.4	0.6	3.4	0.5	49			C1
13	4025.5	0.2	1.8	0.2	51			
14	4036.4	0.3	2.9	0.3	53			
15	4046.1	0.2	1.9	0.2	54	Fe II(2344)	0.7260	
16	4052.4	0.2	1.3	0.2	54			
17	4058.9	0.4	1.1	0.2	54	N V(1238)	2.2765	
18	4072.4	0.3	1.5	0.2	55	N V(1242)	2.2768	
19	4076.5	0.2	1.1	0.2	55			
20	4093.8	0.4	1.4	0.2	56			
21	4109.4	0.4	1.3	0.3	58			C2
22	4112.8	0.3	2.5	0.4	59	Fe II(2382)	0.7261	C2
23	4117.8	0.2	2.1	0.2	60			
24	4129.8	0.2	4.4	0.4	62	H I(1215)	2.3972	
25	4134.8	0.3	1.3	0.1	62			
26	4138.4	0.2	2.2	0.2	63			
27	4152.8	0.2	2.0	0.2	63			
28	4163.0	0.2	1.6	0.2	64			
29	4170.1	0.3	2.9	0.3	64			
30	4179.8	0.4	1.8	0.2	65			
31	4185.5	0.2	4.1	0.4	65			
32	4190.5	0.2	1.0	0.1	66			
33	4199.6	0.3	0.7	0.1	67			
34	4233.0	0.3	2.5	0.2	72			
35	4257.6	0.2	3.8	0.4	78			
36	4261.6	0.4	1.0	0.1	79			
37	4265.8	0.2	0.9	0.1	79			
38	4270.2	0.3	0.6	0.1	81			
39	4280.2	0.2	3.4	0.3	84			
40	4287.7	0.2	1.1	0.1	87			
41	4301.0	0.2	3.3	0.3	91			
42	4312.9	0.2	2.2	0.2	94			
43	4333.0	0.2	0.9	0.1	103			
44	4336.2	0.2	1.0	0.1	105			
45	4345.9	0.2	1.9	0.2	123			
46	4357.4	0.4	1.9	0.3	119			C3
47	4360.5	0.4	1.2	0.2	123			C3
48	4371.7	0.4	1.6	0.2	122,132			
49	4381.6	0.2	1.0	0.1	141,149			
50	4394.3	0.3	0.6	0.1	158,174			
51	4398.0	0.3	2.4	0.3	164,182			
52	4408.2	0.3	4.6	0.4	176,213			
53	4421.1	0.3	4.8	0.7	254,288			C4
54	4425.4	0.5	1.4	0.3	266,323			C4

4. W_2 systems must have the Mg II λλ2796, 2803 lines visible longward of the Lα emission line, both members with $W_{rest} \geq 0.5$ Å; Mg II λ2796 must be stronger than Mg II λ2803. Also, ≥ 1 other lines must be found.

We note that a system may be both S and W and that, with data of the quality used here, the probability that a W system is spurious is $\lesssim 1\%$ (see Paper I). Our definitions lead to well-defined "windows" over which a system can be detected if it is present. The windows for the present QSO data are given in Table 7; it may be seen that the S systems have larger windows than the W systems, as expected.

TABLE 4—*Continued*

n	λ(Å)	σ(λ)Å	W(Å)	σ(W)Å	N_c	Identification	z_{abs}	Comments
55	4429.3	0.3	0.3	0.1	302,350			
56	4433.3	0.3	1.0	0.1	350,407			
57	4437.6	0.3	1.9	0.2	405,482			
58	4464.9	0.2	1.3	0.1	314,396	Fe II(2586)	0.7261	
59	4474.0	0.3	0.4	0.1	249,315	Fe II(2344)	0.9085	
60	4488.0	0.2	2.0	0.2	188.247	Fe II(2600)	0.7260	
61	4547.6	0.2	0.6	0.1	222	Fe II(2382)	0.9086	
62	4566.6	0.2	1.1	0.1	163	Si IV(1393)	2.2765	
63	4596.4	0.4	0.8	0.1	141	Si IV(1402)	2.2766	
64	4826.9	0.2	2.5	0.2	96,65	Mg II(2796)	0.7261	
65	4839.3	0.2	1.9	0.2	93,66	Mg II(2803)	0.7261	
66	4924.5	0.2	1.2	0.1	73	Mg I(2852)	0.7261	
67	5039.0	0.3	4.4	0.6	76	Fe II(2344)	1.1496	C5
68	5043.8	0.5	1.4	0.3	76	Fe II(2344)	1.1516	C5
69	5072.3	0.2	2.2	0.2	81	C IV(1548)	2.2762	
70	5081.0	0.2	1.8	0.2	86	C IV(1550)	2.2764	
71	5104.1	0.2	3.6	0.4	90	Fe II(2374)	1.1496	
72	5122.2	0.3	5.0	0.6	89	Fe II(2382)	1.1496	C6
73	5126.6	0.5	2.5	0.4	89	Fe II(2382)	1.1515	C6
74	5258.5	0.2	1.3	0.1	66	C IV(1548)	2.3966	
75	5266.8	0.2	0.9	0.2	66	C IV(1550)	2.3963	
76	5337.6	0.2	2.1	0.2	63	Mg II(2796)	0.9088	
77	5351.5	0.2	2.0	0.2	61	Mg II(2803)	0.9088	

Notes: (1) Wavelength region analyzed, 3900 Å - 5410 Å.

(2) Other notes as in Table 3.

We also calculated a formal statistical reliability estimate of the reality of the absorption-line systems. This is as described in Paper I, and will be discussed briefly here. Suppose we have a line acceptance "window" of $\Delta\lambda(=0.6$ Å here), and that Δ_J and Δ_L are mean separations in wavelength between lines shortward and longward, respectively, of the Lα emission line. Defining $\rho_J = 2\Delta\lambda/\lambda\Delta_J$ and $\rho_L = 2\Delta\lambda/\Delta_L$, suppose that out of a standard line list, J_1 lines shortward of Lα emission are found (and J_2 are not found), and that L_1 lines longward of Lα emission are also found (and L_2 are not), then we define

$$p(L_1, L_2; \rho_L) = \frac{(L_1 + L_2)!}{L_1!L_2!}\,\rho_L{}^{L_1}(1 - \rho_L)^{L_2}\,, \tag{1}$$

and

$$P = \sum_{J \geq J_1} p(J, J_1 + J_2 - J; \rho_J) \sum_{L \geq L_1} p(L, L_1 + L_2 - L; \rho_L)\,. \tag{2}$$

The probability that the system is spurious based on wavelength coincidence only is $P_1 = PN_b$, where $N_b = (\lambda_{max} - \lambda_{min})/(2\Delta\lambda)$ is the number of independent elements over which the system may occur; λ_{max} and λ_{min} are the edges of the "window" for the system. As described in Paper I, $P_2 = fP_1$, where f is a factor allowing for certain well-defined physical criteria which must be satisfied. In Table 8, we present all these values. Multiplying these probabilities, we find that the systems of Tables 5 and 6 have a probability greater than 95% of being real. Despite there being a number of three- and four-line systems, this value is high because of our stringent requirements in wavelength and relative equivalent widths, especially for members of close doublets.

In both QSOs, all lines longward of the Lα emission line were successfully identified (there being 18 such lines in Q0002−422 and 20 in Q0453−423), whereas only a small fraction of those shortward of Lα could be identified (14 out of 62 in Q0002−422 and seven out of 57 in Q0453−423). The unidentified lines shortward of Lα emission were investigated in PKS 2126−158 (Paper I), and, by cross-correlating appropriate regions of spectrum, it was found that most of the lines were Lα absorption in systems so weak that no other lines (including Lβ) were visible. Moreover, a histogram of line-pair separations showed that no more than a few (~3) C IV or Mg II doublets could be present among the lines shortward of Lα. The two QSOs considered here were not observed at short enough wavelengths to allow a Lα/Lβ analysis similar to that performed on the PKS 2126−158 data. However, in Figures 3 and 4, we present the line separation plots which again show that only very few C IV or Mg II doublets could be present shortward of Lα.

TABLE 5

Q0002−422: Absorption-Line Systems

	Ion	Rest λ (Å)	λ(1+z_{abs}) (Å)	Obs. λ (Å)	O-C (Å)	(1+z_{abs})	W (Å)	W/(1+z) (Å)	Comments
1	MgI	2852.97	5239.88	5239.63	-0.26	0.8365	2.5	1.4	
	MgII(1)	2803.53	5149.08	5149.00	-0.08	0.8366	7.4	4.0	
	MgII(2)	2796.35	5135.89	5135.40	-0.49	0.8365	8.6	4.7	
	FeI	2719.81	4995.20	...	...	...	<0.8	<0.4	
	FeII(J=9/2)	2600.18	4775.60	4775.83	+0.23	0.8367	5.4	2.9	
	FeII	2586.64	4750.73	4750.92	+0.19	0.8367	3.1	1.7	
	FeII	2382.76	4376.27	4376.35	+0.08	0.8367	5.1	2.8	
	FeII	2374.46	4360.93	4361.21	+0.28	0.8367	2.4	1.3	Sum of lines 42 and 43
	FeII	2367.59	4348.32	...	...	...	<0.7	<0.4	
	FeII	2344.21	4305.47	4306.64	+1.16	0.8371	2.7	1.5	Blended with SiIV(1304) of z_{abs} = 2.3018
	FeII*(J=3/2)	2631.83	4833.62	...	...	...	<1.0	<0.5	
	FeII*(J=1/2)	2629.07	4828.55	...	...	...	<1.5	<0.8	
	FeII*(J=7/2)	2612.65	4798.39	...	...	...	<1.0	<0.5	
	FeII*(J=5/2)	2607.87	4789.61	...	...	...	<1.0	<0.5	
					$\langle z_{abs} \rangle$ = 0.8366				
2	CIV(1)	1550.77	4634.58	4634.60	+0.02	1.9886	1.9	0.64	
	CIV(2)	1548.20	4626.90	4626.90	0.00	1.9886	2.2	0.74	
	SiII	1526.72	4562.71	4562.69	-0.02	1.9886	0.5	0.17	
					$\langle z_{abs} \rangle$ = 1.9886				
3	HI	1215.67	3851.59	3851.85	+0.26	2.1685	3.6	1.1	
	CIV(1)	1550.77	4913.28	4913.16	-0.12	2.1682	0.9	0.28	
	CIV(2)	1548.20	4905.14	4904.95	-0.19	2.1682	1.1	0.35	
					$\langle z_{abs} \rangle$ = 2.1683				
4	HI	1215.67	4013.99	4013.98	+0.01	2.3019	5.9	1.8	
	CII(J=1/2)	1334.53	4406.44	4406.05	-0.39	2.3016	3.4	1.0	
	CII*(J=3/2)	1335.68	4410.23	...	...	...	<1.5	<0.5	
	CIV(1)	1550.77	5120.44	5120.40	-0.04	2.3018	2.8	0.85	
	CIV(2)	1548.20	5111.94	5111.89	-0.05	2.3018	3.8	1.4	
	OI	1302.17	4299.59	4299.23	-0.36	2.3016	0.9	0.27	
	SiII(J=1/2)	1526.72	5041.03	5040.88	-0.15	2.3018	1.6	0.48	
	SiII*(J=3/2)	1533.44	5063.21	...	...	...	<1.0	<0.3	
	SiII	1304.37	4306.86	4306.64	-0.22	2.3017	2.7	0.82	Blended with FeII(2344)
	SiII*	1309.28	4323.07	...	...	...	<0.8	<0.2	of z_{abs} = 0.8366
	SiII	1260.42	4161.74	4161.91	+0.17	2.3020	2.1	0.63	
	SiII*	1265.04	4176.99	...	...	...	<1.0	<0.3	
	SiII(2)	1193.28	3940.05	3940.27	+0.22	2.3021	2.4	0.73	
	SiII(1)	1190.42	3930.61	3930.17	-0.45	2.3015	2.3	0.70	
	SiII*	1197.42	3953.72	...	...	...	<1.0	<0.3	
	SiII*	1194.50	3944.08	...	...	...	<1.0	<0.3	
	SiIII	1206.51	3983.73	3938.48	-0.25	2.3017	3.1	0.94	
	SiIV(1)	1402.77	4631.76	4632.00	+0.24	2.3020	2.5	0.76	
	SiIV(2)	1393.76	4602.01	4602.20	+0.19	2.3020	3.0	0.91	
					$\langle z_{abs} \rangle$ = 2.3018				
5	HI	1215.67	4211.14	4211.32	+0.18	2.4642	6.2	1.8	
	CIV(1)	1550.77	5371.94	5371.45	-0.49	2.4637	1.9	0.55	
	CIV(2)	1548.20	5363.04	5362.55	-0.49	2.4637	2.5	0.72	
	SiIV(1)	1402.77	4859.26	4859.75	+0.49	2.4644	0.8	0.23	
	SiIV(2)	1393.76	4828.05	4828.54	+0.49	2.4644	1.2	0.34	
					$\langle z_{abs} \rangle$ = 2.4641				

TABLE 6

Q0453−423: Absorption-Line Systems

	Ion	Rest λ (Å)	λ(1+z_{abs}) (Å)	Obs. λ (Å)	O-C (Å)	(1+z_{abs})	W (Å)	W/(1+z) (Å)	
1	MgI	2852.97	4924.53	4924.45	-0.09	0.7261	1.2	0.70	
	MgII(1)	2803.53	4839.18	4839.32	+0.14	0.7261	1.9	1.1	
	MgII(2)	2796.35	4826.79	4826.92	+0.13	0.7261	2.5	1.4	
	FeI	2523.61	4356.00	...	...	...	<0.5	<0.3	
	FeI	2484.02	4287.67	...	...	...	<0.5	<0.3	
	FeII(J=9/2)	2600.18	4488.19	4488.02	-0.17	0.7260	2.0	1.2	
	FeII	2586.64	4464.82	4464.91	+0.09	0.7261	1.3	0.75	
	FeII	2382.76	4112.87	4112.82	-0.05	0.7261	2.5	1.5	
	FeII	2374.46	4098.56	...	...	...	<0.7	<0.4	
	FeII	2344.21	4046.33	4046.10	-0.22	0.7260	1.9	1.1	
	FeII*(J=3/2)	2631.83	4542.80	...	...	...	<0.3	<0.17	
	FeII*(J=1/2)	2629.07	4538.04	...	...	...	<0.3	<0.17	
	FeII*(J=7/2)	2612.65	4509.70	...	...	...	<0.3	<0.17	
	FeII*(J=5/2)	2607.87	4501.44	...	...	...	<0.3	<0.17	
					$\langle z_{abs} \rangle$ = 0.7261				
2	MgII(1)	2803.53	5351.16	5351.46	+0.30	0.9088	2.0	1.1	
	MgII(2)	2796.35	5337.45	5337.56	+0.11	0.9088	2.1	1.1	
	FeII(J=9/2)	2382.76	4548.03	4547.64	-0.40	0.9086	0.6	0.32	
	FeII	2344.21	4474.45	4474.02	-0.43	0.9085	0.4	0.21	
					$\langle z_{abs} \rangle$ = 0.9087				
3a	FeII(J=9/2)	2382.76	5121.91	5122.19	+0.19	1.1496	5.0	2.3	
	FeII	2374.46	5104.07	5104.07	-0.07	1.1496	3.6	1.7	
	FeII	2367.59	5089.37	...	...	...	<0.7	<0.3	
	FeII	2344.21	5039.04	5039.07	+0.03	1.1496	4.4	2.0	
	FeII*(J=1/2)	2411.79	5184.31	...	...	...	<0.8	<0.4	
	FeII*(J=3/2)	2411.25	5183.15	...	...	...	<0.8	<0.4	
	FeII*(J=5/2)	2406.61	5173.18	...	...	...	<0.8	<0.4	
	FeII*(J=7/2)	2396.36	5151.14	...	...	...	<0.8	<0.4	
					$\langle z_{abs} \rangle$ = 1.1496				
3b	FeII(J=9/2)	2382.76	5126.66	5126.60	-0.06	1.1515	2.5	1.2	
	FeII	2374.46	5108.89	...	...	...	<0.8	<0.4	
	FeII	2344.21	5043.72	5043.77	+0.05	1.1516	1.4	0.65	
					$\langle z_{abs} \rangle$ = 1.1516				
4	HI	1215.67	3983.14	3983.08	-0.06	2.2764	4.2	1.3	
	CII	1334.53	4372.59	...	...	...	<0.8	<0.25	
	CIV(1)	1550.77	5081.10	5080.99	-0.11	2.2764	1.8	0.55	
	CIV(2)	1548.20	5072.68	5072.28	-0.40	2.2762	2.2	0.67	
	NV(1)	1242.80	4072.03	4072.41	+0.38	2.2768	1.5	0.46	Probably blended
	NV(2)	1238.81	4058.96	4058.91	-0.05	2.2765	1.1	0.34	
	SiII	1193.28	3909.78	...	...	...	<1.0	<0.3	
	SiIII	1206.51	3953.13	3953.38	+0.25	2.2767	1.6	0.49	
	SiIV(1)	1402.77	4596.18	4596.35	+0.17	2.2766	0.8	0.24	
	SiIV(2)	1393.76	4566.65	4566.64	-0.01	2.2765	1.1	0.34	
					$\langle z_{abs} \rangle$ = 2.2765				
5	HI	1215.67	4129.27	4129.82	+0.55	2.3972	4.4	1.3	
	CIV(1)	1550.77	5267.50	5266.84	-0.66	2.3963	0.9	0.27	
	CIV(2)	1548.20	5258.77	5258.54	-0.23	2.3966	1.3	0.38	
					$\langle z_{abs} \rangle$ = 2.3967				

TABLE 7

ABSORPTION-LINE SYSTEM VISIBILITY WINDOWS

Type of System	No. of Systems	z_{min}	z_{max}	Δz
Q0002−422:				
S_1.....	1	2.094	2.882	0.788
W_1.....	4	1.871	2.488	0.617
S_2.....	1	0.469	1.084	0.615
W_2.....	1	0.589	0.929	0.340
Others.....	0	...	...	...
Q0453−423:				
S_1.....	0	2.015	2.889	0.874
W_1.....	2	1.955	2.495	0.540
S_2.....	1	0.508	1.081	0.573
W_2.....	2	0.636	0.933	0.297
Others.....	1	...	...	...

b) Redshift Systems and Column Densities

In this section, we discuss the line identifications and column densities for the individual redshift systems. The column densities given in Tables 9 and 10 are generally calculated assuming that the velocity distribution of material along the line of sight is Gaussian, $N(v) = N_0 \exp(-v^2/2\sigma_v^2)$, or, if the system is clearly split, a sum of several Gaussians. An appropriate curve of growth (including damping) was calculated numerically from the velocity model for which the column densities were obtained. We stress that this procedure will yield only estimates of the column densities because such determinations are very ill-conditioned mathematically whenever the instrumental resolution exceeds the natural broadening width of the lines in question. Because of this, in Tables 9 and 10 we decline to give error estimates based on the statistical errors in the equivalent widths of the absorption lines; such errors of 10% would give a misleading impression of the accuracy of the column densities.

We must draw particular attention to the following points:

1. A curve-of-growth analysis cannot be performed on the Si II lines because of the poor condition of their oscillator strengths. The tabulated values (Morton and Smith 1973) do not agree with the observed line strengths (see, e.g., Morton 1975). We have used, where possible, the Si II λλ1190, 1193 lines with *f*-values as given in Morton (1978).

2. In the unresolved systems where a single Gaussian model was employed, errors will arise when saturated, low-dispersion components are present. Boksenberg, Carswell, and Sargent (1979) illustrate the errors possible even in very high-resolution data.

Comments on the individual systems are as follows:

1. Q0002−422; $z_{abs} = 0.8366$. This system was recognized, with five lines, by WCS. We have added three Fe II lines to make this system, with $z_{abs} \ll z_{em}$ (corresponding to $v/c = 0.615$), indisputable. It is a strong, split system

TABLE 8

STATISTICAL ANALYSIS OF ABSORPTION-LINE SYSTEMS

QSO	z_{abs}	Type of System	M_1	M_2	N_1	N_2	N_b	P	P_1	P_2
Q0002-422	0.8366	S_2,W_2	2	1	5	0	2000	8×10^{-11}	2×10^{-7}	3×10^{-8}
ρ_m=0.0800	1.9886	W_1	1	1	2	0	845	2×10^{-4}	2×10^{-1}	2×10^{-2}
ρ_n=0.0213	2.1683	W_1	1	0	2	1	845	7×10^{-5}	6×10^{-2}	1×10^{-2}
	2.3018	S_1,W_1	7	0	5	0	1080	9×10^{-17}	1×10^{-14}	3×10^{-16}
	2.4641	W_1	1	0	2	1	845	1×10^{-4}	9×10^{-2}	1×10^{-2}
Q0453-423	0.7261	S_2,W_2	2	1	5	0	1862	7×10^{-11}	1×10^{-7}	1×10^{-9}
ρ_m=0.1046	0.9087	W_2	0	4	4	0	965	2×10^{-7}	2×10^{-4}	2×10^{-5}
ρ_n=0.0207	{1.1496 1.1516}*	...	0	0	3	0	900	9×10^{-6}	8×10^{-3}	1×10^{-3}
	2.2765	W_1	2	1	4	0	965	5×10^{-9}	5×10^{-6}	2×10^{-7}
	2.3967	W_1	1	0	2	1	965	1×10^{-4}	1×10^{-1}	1×10^{-2}

*This system is undoubtedly real. Five additional lines are to be found in CSW, outside our observed region.

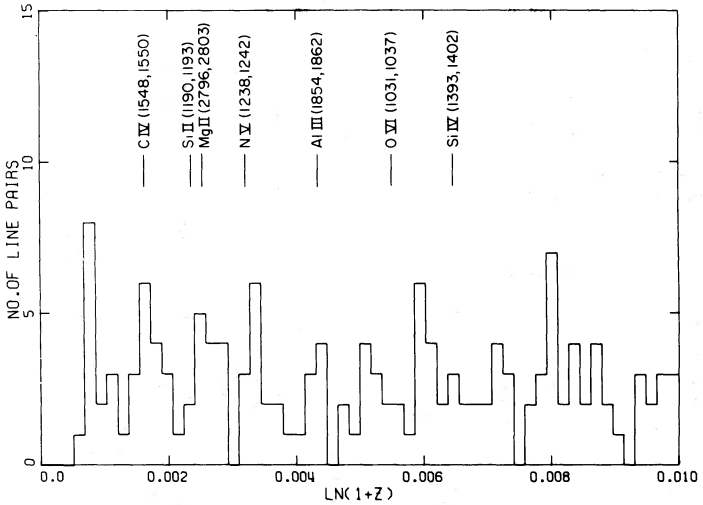

FIG. 3.—Distribution of splittings $\Delta \ln (1 + z) = |\ln (\lambda_1/\lambda_2)|$ among pairs of unidentified absorption lines in the spectrum of Q0002−422. The positions of seven line pairs, often found in QSO spectra, are marked.

with at least two components. Examination of the Fe II λλ2374, 2382, 2586 lines shows two components; the Fe II λ2600 line suggests a third component which is not supported by the other lines. The Fe II line profiles were fitted by a two-cloud model separated by 160 km s^{-1}; the blueward cloud has a dispersion of 50 km s^{-1} and the redward cloud of 35 km s^{-1}. The total column densities are in the ratio 1.79:1, with the blue cloud stronger. A curve of growth with this model was used to generate the column densities given in Table 9; this curve is shown in Figure 5. The coordinates used are log W/b_λ, where W is the equivalent width of the line and b_λ is the wavelength increment corresponding to 50 km s^{-1} (an arbitrary scaling parameter). Also, log τ_0 is used, where τ_0 is the optical depth in the indicated position of the complex line structure. With these coordinates, the column density is $N_i = K\tau_0 b_\lambda W_0^{-1}$, where $W_0 = (\pi e^2/m_e c^2) f\lambda^2$, and $K = 3.91$ [instead of $(2\pi)^{1/2}$, as it would be for a Gaussian velocity distribution with dispersion b_λ]. Fe II λ2344 is blended and was not used in the analysis.

Column densities for the system are given in Table 9. Because Mg II is on the logarithmic part of the curve of growth, the column density N(Mg II) is rather uncertain.

2. Q0002−422; $z_{abs} = 1.9886$. This is the least probable of any of the systems presented here, having only three lines, among which C IV λ1550 is blended with Si IV λ1402 in the $z_{abs} = 2.3018$ system. There is no doubt as to the reality of any of the lines, and an examination of the Si IV λ1393 line at $z_{abs} = 2.3018$ shows that Si IV λ1402 in this system is certainly blended with another line. The situation is further complicated, however, by the

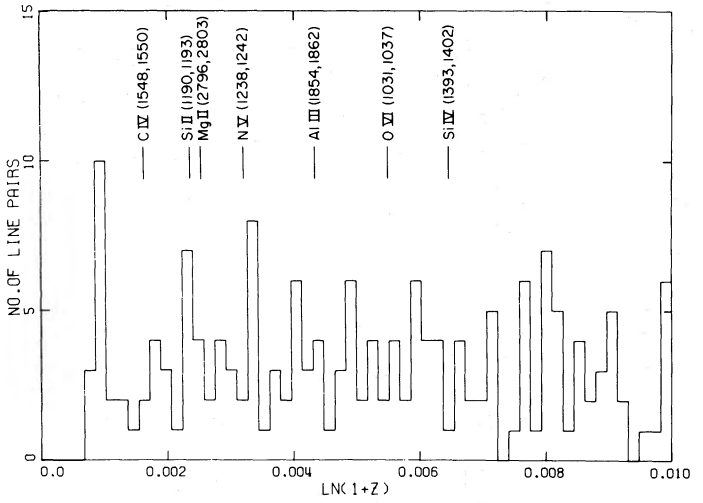

FIG. 4.—Distribution of splittings $\Delta \ln (1 + z) = |\ln (\lambda_1/\lambda_2)|$ among pairs of unidentified absorption lines in the spectrum of Q0453−423. The positions of seven line pairs, often found in QSO spectra, are marked.

TABLE 9

Q0002−422: COLUMN DENSITIES

ION	z_{abs} 0.8366†	1.9886	2.1683‡	2.3018		2.4641
σ_v (km s^{-1})	35, 50	50	{15 / 4.7}	40:	65	37
H I	...	...	{2×10^{18} / 3×10^{18}}	2×10^{18}	...	3×10^{18}
C II ($J = 1/2$)	...	...	...	7×10^{15}:	...	...
C II* ($J = 3/2$)	...	...	...	$< 5 \times 10^{14}$	...	...
C IV	...	3×10^{14}	{4×10^{14} / 3×10^{17}}	...	7×10^{14}	5×10^{14}
O I	...	...	...	5×10^{14}:	...	...
Mg I	1.4×10^{13}	...	...	...	...	...
Mg II	1.6×10^{16}:	...	...	...	...	...
Si II ($J = 1/2$)§	...	$9 \times 10^{13} F_{1526}{}^{-1}$	...	7×10^{14}:	...	...
Si II* ($J = 3/2$)	...	...	...	$< 5 \times 10^{13}$	...	...
Si III	...	...	...	...	1.1×10^{14}	...
Si IV	...	...	...	...	2×10^{14}	6×10^{13}
Fe I	$< 7 \times 10^{13}$	...	...	...	...	...
Fe II ($J = 9/2$)	8×10^{14}	...	...	...	...	...
Fe II* ($J = 7/2$)	$< 8 \times 10^{13}$	...	...	...	...	...
Fe II*($J = 5/2$)	$< 8 \times 10^{13}$	...	...	...	...	...
Fe II* ($J = 3/2$)	$< 8 \times 10^{13}$	...	...	...	...	...
Fe II* ($J = 1/2$)	$< 9 \times 10^{13}$	...	...	...	...	...

† Two-cloud model, see § III*b*.

‡ Two solutions possible; both are given.

§ Oscillator strengths for this ion uncertain: f_{1526} = oscillator strength of Si II λ1526; $F_{1526} = f_{1526}/0.1$.

possible presence at this wavelength of Fe I λ2523 from the strong system $z_{abs} = 0.8366$. Si IV λ1393 is not visible, despite the reasonable strength of C IV, nor is C II λ1334, despite the presence of Si II λ1526.

The Si II λ1526 line is unsaturated (since it is shallow and much broader than the instrumental resolution; we appreciate that this is not the case if dense, narrow, multiple clouds are invoked) and gives a dispersion $\sigma_v = 44$ km s^{-1}. The C IV doublet ratio cannot be used since the lines are confused, but the width of the C IV λ1548 line is $\sigma_v = 60$ km s^{-1}. Because this line is rather deep, the ionic dispersion $\sigma_v < 60$ km s^{-1} for C IV. We shall adopt $\sigma_v = 50$ km s^{-1} for the calculation of the column densities in Table 9.

3. Q0002−422; $z_{abs} = 2.1683$. This is a possible system based on C IV λλ1548, 1550 and Lα. The C IV doublet is rather weak, with a ratio $R = 1.22$. This admits two possible solutions for the column density and velocity dispersion of C IV ions:

a) Lines on the logarithmic part of the curve of growth. Then we find $\sigma_v = 15$ km s^{-1} and N(C IV) $= 4 \times 10^{14}$ cm^{-2}.

TABLE 10

Q0453−423: COLUMN DENSITIES

ION	z_{abs} 0.7261	1.1496	1.1516	2.2765	2.3967
σ_v (km s^{-1})	41	50	70	25	23
H I	...	...	...	2×10^{18}	2×10^{18}
C II	...	...	...	$< 2 \times 10^{14}$	...
C IV	...	...	...	9×10^{14}	2×10^{14}
N V	...	...	...	4×10^{14}	...
Mg I	7×10^{12}	1.0×10^{13}		...	...
Mg II	1.0×10^{14}	4×10^{15}		...	...
Si II	...	...	...	$< 8 \times 10^{13}$	...
Si III	...	...	...	1.4×10^{14}	...
Si IV	...	...	...	7×10^{13}	...
Fe I	$< 1.8 \times 10^{13}$	...	...	...	...
Fe II ($J = 9/2$)	4×10^{14}	2×10^{15}	1.3×10^{14}	...	...
Fe II* ($J = 7/2$)	$< 3 \times 10^{13}$	$< 3 \times 10^{13}$	...	...	...
Fe II* ($J = 5/2$)	$< 4 \times 10^{13}$	$< 3 \times 10^{13}$	...	...	...
Fe II* ($J = 3/2$)	$< 3 \times 10^{13}$	$< 4 \times 10^{13}$	...	...	...
Fe II* ($J = 1/2$)	$< 2 \times 10^{13}$	$< 4 \times 10^{13}$	...	...	...

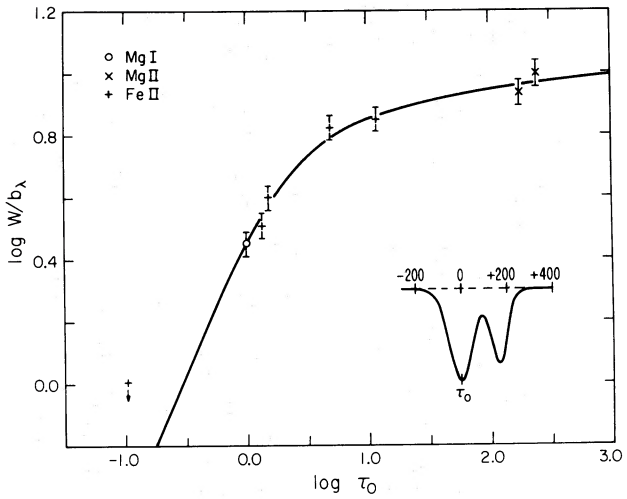

FIG. 5.—Curve of growth for system $z_{abs} = 0.8366$ in Q0002−422 for lines of Mg I, Mg II, and Fe II. A complex line profile as shown was used to generate the curve (the velocity scale on the line profile is in km s^{-1}). The quantity τ_0 is the optical depth at the indicated point in the line. W is the equivalent width of the line in units of b_λ corresponding to 50 km s^{-1} at the wavelength of the line.

b) Lines on the square root part of the curve of growth. With this hypothesis, $\sigma_v = 4.7$ km s^{-1} and N(C IV) = 3×10^{17} cm^{-2}.

The lines are sufficiently narrow and ill-resolved that we would not expect to see the strong damping wings characteristic of solution (*b*); we therefore cannot distinguish between the two cases. Slightly different column densities for H I result from the two dispersions of (*a*) and (*b*); these are given in Table 9.

4. Q0002−422; $z_{abs} = 2.3018$. A certain system in which seven lines were noted by WCS. These included a line observed outside our range, at λ5511.5, which they identified as Al II λ1670. This is a very typical S_1 system, with C II, C IV, Si II, Si III, and Si IV among the metals, but with no excited fine-structure states C II* or Si II*. The Si II λ1304 line is blended with Fe II λ2344 in $z_{abs} = 0.8366$, and the Si II λ1193 line is severely confused.

There is a difference in dispersion (and mean redshift) between the low- and high-ionization material. Inspection of the C IV λλ1548, 1550, Si IV λ1393, and Si III λ1206 lines shows a higher dispersion than for C II λ1334, O I λ1302, or Si II λλ1190, 1260, 1526. The C IV doublet ratio R(C IV) = 1.36 gives $\sigma_v = 65$ km s^{-1} (we exclude the damped solution for this doublet ratio, which fails to show the appropriate strong wings, although detection of such wings can be much harder if appropriately perverse multiple cloud models are invoked). Because the λ1402 line of the Si IV doublet is confused and the Si III line is saturated, this is the only dispersion estimate available. This dispersion is used to calculate the column densities in C IV, Si III, and Si IV (from the λ1393 line), which are given in Table 9.

It is not possible to calculate accurately the dispersion in the low-ionization material because of the sorry condition of the Si II oscillator strengths. The only unsaturated, unconfused lines are O I λ1302 and Si II λ1526. These give $\sigma_v = 25$ km s^{-1} and 44 km s^{-1}, respectively. Since the O I identification is not a certain one (only one line from that ion), we adopt, with great uncertainty, a value $\sigma_v = 40$ km s^{-1}. The column densities for C II, O I, and Si II are given in Table 9, with the value of N(Si II) based on λ1190.

5. Q0002−422; $z_{abs} = 2.4641$. A probable five-line system with H I, C IV, and Si IV. The absence of Si III and C II shows that this system has a moderately high ionization. There is a peculiar disparity in shape for the Si IV λλ1393, 1402 doublet. The λ1402 line is broad and shallow, whereas the λ1393 line is deep and sharp, although the doublet ratio R(Si IV) = 1.50 is reasonable. This suggests unfortunate fluctuations in the noise in one or both of the lines.

The C IV λλ1548, 1550 doublet ratio is R(C IV) = 1.32, which admits two solutions for the velocity dispersion and column density. The damped solution may be excluded by the line profiles which fail to show the strong wings expected of a Lorentzian profile. The dispersion is $\sigma_v = 37$ km s^{-1} from C IV, which is consistent with a dispersion $\sigma_v = 39$ km s^{-1} of the unsaturated Si IV λ1402 line. This does not agree with the width of the Si IV λ1393 line, which has a dispersion $\sigma_v = 17$ km s^{-1} (after correction for instrumental resolution). The line, however, is too deep for its width, after allowing for resolution effects, and we therefore suspect the Si IV λ1393 of being the deviant.

Using the dispersion $\sigma_v = 37$ km s^{-1}, we may calculate the column densities given in Table 9. The value for Si IV was derived from the Si IV λ1402 line.

6. Q0453−423: $z_{abs} = 0.7261$. This is a strong system with $z_{abs} \ll z_{em}$ (corresponding to $v/c = 0.635$), which was suggested by CSW on the basis of an Mg II doublet only. With seven lines, it is now a certain system with the usual manifestation of Mg I, Mg II, and Fe II, but no Fe I or Fe II*.

The Mg II λλ2796, 2803 doublet ratio R(Mg II) = 1.32 gives a velocity dispersion σ_v = 40 km s^{-1} (the damped solution corresponding to this ratio was rejected on the basis of the line profiles). A full curve-of-growth analysis, including the Mg II and Fe II lines, gave σ_v = 41 km s^{-1} and the column densities shown in Table 10.

7. Q0453−423; z_{abs} = 0.9087. A probable Mg II, Fe II system with four lines. This was also noted by CSW, but they included the Fe II λ2600 line observed at 4961.3 Å which was not acceptable as a line in our data.

The Mg II λλ2796, 2803 doublet ratio is very low, R(Mg II) = 1.05, which is the lowest possible value for a damping parameter $a = \lambda_0\Gamma/4\pi\sigma_v = 3.5 \times 10^{-4}$. This gives a rather low dispersion σ_v = 16 km s^{-1}, but is very uncertain because of possible errors in the doublet ratio. Because column densities in this situation are uncertain by a factor of ∼30, we decline to present any values.

8. Q0453−423; z_{abs} = 1.1496, 1.1516. This is a very strong S_2 system. (SW report five lines of Fe II, Mg II, Mg I outside the range of our observations.) The system is double, with a splitting of 280 km s^{-1}. The higher redshift component, visible on the wings of the lower redshift system, is seen in Fe II λλ2344, 2382 but not in Fe II λ2374. The stronger system is seen in Fe II λλ2344, 2374, 2382 but not in Fe II λ2367. The line profiles were fitted by two Gaussian components with σ_v = 50 km s^{-1} for the strong component and 70 km s^{-1} for the weak component. The column densities are in the ratio 1:0.060. For Fe II, it was possible to calculate the column densities in the systems separately. We took the equivalent widths of Mg I λ2852 and Mg II λλ2796, 2803 from CSW as 2.1 Å, 11.7 Å, and 10.6 Å, respectively (a multiplicative factor obtained from the Fe II lines was used to bring the CSW values into agreement with those in Table 6). This enabled us to compute the total column density in Mg I and Mg II assuming the same velocity model as was found for Fe II.

9. Q0453−423; z_{abs} = 2.2765. A strong, high-redshift system with eight lines, of which five were noted by CSW. We have added the Si III λ1206 line and the N V λλ1238, 1242 doublet to this system. It is a system with moderately high ionization conditions, as evidenced by the lack of C II and Si II (Si II λ1260 would be blended with Lα at z_{abs} = 2.3967, but Si II λ1193 is not present in our data, and the C II λ1334 identification leads to an unacceptable wavelength residual of 1 Å). The N V λ1242 line is probably blended with another weak line since it is stronger than the N V λ1238 line.

The C IV doublet ratio is R(C IV) = 1.22, which gives σ_v = 29 km s^{-1} (the damped solution cannot be reconciled with the observed line profiles). The Si IV doublet ratio is R(Si IV) = 1.38, which gives σ_v = 21 km s^{-1}. We thus adopt σ_v = 25 km s^{-1}. The column densities are given in Table 10; we use the N V λ1238 line since the λ1242 line may be blended.

10. Q0453−423; z_{abs} = 2.3967. A probable system with the C IV doublet and H I, as suggested by CSW. We reject their identification of Si II λ1260 in this system because of the large wavelength discrepancy. The C IV doublet ratio is R(C IV) = 1.44, which gives a dispersion σ_v = 23 km s^{-1}. The errors in R(C IV) would admit the possibility of a solution on the damping part of the curve of growth which is excluded by the absence of strong wings. The column densities of C IV and H I are given in Table 10.

Finally, we note that the possible system z_{abs} = 2.2046, suggested by CSW, is not supported by the present data.

IV. THE ORIGIN OF THE ABSORPTION SYSTEMS

a) Mean Free Path Between Absorbing Clouds

Our well-defined criteria for identifying specified types of redshift system from uniform data allow us to compare the results for different QSOs with relative freedom from selection effects. We first examine the distributions of the different types of redshift in the three QSOs PKS 2126−158, Q0002−422, and Q0453−423 on the hypothesis that the redshift systems arise in intervening galaxies. Table 11 contains information on the density of absorption-line systems of the various types defined in § II*a*.

TABLE 11

DENSITY OF ABSORPTION-LINE SYSTEMS

System	Q0002−422	Q0453−423	PKS 2126−158	Mean
S_1:				
$\langle z_{abs}\rangle$.....	2.488	2.452	2.786	2.575
$N(z)$*.....	1.27 (1)	0 (0)	2.02 (2)	1.10 (3)
W_1:				
$\langle z_{abs}\rangle$.....	2.179	2.225	2.820	2.408
$N(z)$*.....	6.48 (4)	3.70 (2)	3.26 (3)	4.48 (9)
S_2:				
$\langle z_{abs}\rangle$.....	0.777	0.794	1.110	0.894
$N(z)$*.....	1.63 (1)	1.75 (1)	0 (0)	1.13 (2)
W_2:				
$\langle z_{abs}\rangle$.....	0.759	0.784	1.143	0.895
$N(z)$*.....	2.94 (1)	6.73 (2)	0 (0)	3.22 (3)

* Number of redshift systems per unit interval Δz = 1. Numbers in parentheses give the number of systems occurring in that QSO.

The mean free path for intercepting an absorbing cloud is

$$\lambda = (c\Delta z/H_0)(1 + z)^{-2}(1 + 2q_0z)^{-1/2}, \tag{3}$$

where Δz is the mean separation of adjacent absorption redshifts at redshift z. The Schechter (1976) galaxy-luminosity function has been combined with the Holmberg (1976) radius-luminosity relations for galaxies by Burbidge *et al.* (1977) to yield:

Schechter:

$$dn = \phi_*(L/L_*)^{-5/4} \exp(-L/L_*) \quad (\mathrm{Mpc}^{-3}); \tag{4a}$$

$$\phi_* = 4 \times 10^{-2}h_{100}{}^3 \quad (\mathrm{Mpc}^{-3}); \tag{4b}$$

$$M_{B(0)}{}^* = -19.1 + 5 \log h_{100} \quad \text{(for luminosity } L_*); \tag{4c}$$

Holmberg:

$$\sigma = \sigma_*(L/L_*)^{5/6} = \pi R_*{}^2(L/L_*)^{5/6}; \tag{4d}$$

Burbidge *et al.*:

$$\lambda = [\sigma_*\phi_*\Gamma(7/12)]^{-1} = 0.654/\sigma_*\phi_*; \tag{4e}$$

where $h_{100} = H_0/100 \text{ km s}^{-1} \text{ Mpc}^{-1}$, σ is the galactic cross section to absorption (of above a specified column density), and σ_* and R_* are the cross section and radius, respectively, of a galaxy of luminosity L_* (the "fiducial" value in the luminosity function). The Holmberg relations are relevant to the optical size of the galaxy and may not hold for large halos. We shall scale matters by letting $\phi_*(z) = \phi_*(1 + z)^3$; the applicability of the luminosity-radius relations will be assumed for high redshift despite the probability of and uncertain nature of the evolution of galactic halos. Combining equations (3) and (4e) yields,

$$\sigma_* = [\Gamma(7/12)]^{-1}(H_0/c\Delta z\phi_*)(1 + 2q_0z)^{1/2}(1 + z)^{-1}, \tag{5}$$

and so we find

$$R_* = (\sigma_*/\pi)^{1/2} = [\pi\Gamma(7/12)]^{-1/2}[H_0/c\Delta z\phi_*]^{1/2}(1 + 2q_0z)^{1/4}(1 + z)^{-1/2}, \tag{6a}$$

which becomes, numerically,

$$R_* = (41.6 \text{ kpc})\, h_{100}{}^{-1}[(1 + z)\Delta z]^{-1/2}(1 + 2q_0z)^{1/4}. \tag{6b}$$

For the S_1, W_1, S_2, W_2 systems, the values of R_* are 23, 48, 32, and 54 kpc, respectively. If, instead of a spherical absorber, one considers randomly oriented disks, then the required disk radius is simply $R_*(2)^{1/2}$. These lengths seem quite reasonable for putative halos of galaxies with luminosity L_*; galaxies with $M_{B(0)} = -16 + 5 \log h_{100}$ would have $R = 0.3R_*$. The fine splittings, of order 100 km s^{-1}, frequently observed in the heavy-element systems, also point to galactic halos as plausible places of origin (Bahcall 1975; Boroson *et al.* 1978). Lastly, we note that our estimates of R_* are calculated from well-defined samples of redshift systems (previous calculations have used inhomogeneous samples) and that the dependence $R_* \propto h_{100}{}^{-1}$ will raise R_* to the often-quoted value of 100 kpc (for W_1 and W_2 systems) if $H_0 = 50 \text{ km s}^{-1} \text{ Mpc}^{-1}$ is used.

The cosmological density of the absorbing clouds may be calculated. The density of material is given by,

$$\rho_{\text{cloud}} = N(\text{H})m_p/\lambda = N(\text{H I})m_p/\lambda, \tag{7}$$

where $N(\text{H})$ is the column density of one cloud, λ is the mean free path between clouds, and $f = N(\text{H I})/N(\text{H})$. Thus,

$$\rho_{\text{cloud}} = [m_pN(\text{H I})/f](H_0/c\Delta z)(1 + z)^2(1 + 2q_0z)^{1/2}. \tag{8}$$

Dividing by $(1 + z)^3$ to correct to the present epoch, and using $\rho_{\text{crit}} = 3H_0{}^2/8\pi G = 1.9 \times 10^{-29}h_{100}{}^2 \text{ g cm}^{-3}$, we find,

$$\begin{aligned}\Omega_{\text{cloud}} &= [8\pi m_pN(\text{H I})G/3H_0fc\Delta z](1 + z)^{-1}(1 + 2q_0z)^{1/2} \\ &= (2.9 \times 10^{-5}/f\Delta z)[N(\text{H I})/3 \times 10^{18}]h_{100}{}^{-1}(1 + z)^{-1}(1 + 2q_0z)^{1/2}.\end{aligned} \tag{9}$$

For the W_1 systems, the typical column density is $N(\text{H I}) = 3 \times 10^{18} \text{ cm}^{-2}$, the ionization fraction $f = 1/30$ (see below), and Δz is given in Table 11 (for $\langle z \rangle = 2.4$). This gives $\Omega_{\text{cloud}} = 1.3 \times 10^{-3}h_{100}{}^{-1}(1 + 4.8q_0)^{1/2}$ for the W_1 systems. For the W_2 systems, the hydrogen is not in the observable range. The column densities of Mg and Fe

suggest $N(\mathrm{H}) = 10^{20}$ for the W_1 systems (see below); using Table 11, we find $\Omega_{\mathrm{cloud}} = 1.5 \times 10^{-3} h_{100}^{-1}(1 + 1.8q_0)[N(\mathrm{H})/10^{20}\ \mathrm{cm}^2]$. Thus, the required cosmological densities $\Omega_{\mathrm{cloud}} \sim 10^{-3}$ are similar for the W_1 and W_2 systems.

b) Physical Conditions in the Absorbing Gas

i) *The S_1 Systems*

This common type of system is represented by the $z_{\mathrm{abs}} = 2.6381$, 2.7685 redshifts in PKS 2126−158, and by $z_{\mathrm{abs}} = 2.3018$ in Q0002−422. (There are no examples of an S_1 system by the strict definition in Q0453−423.) The line strengths and estimated column densities typical of S_1 systems may be inspected in the relevant tables.

An examination of the work of McKee, Tarter, and Weisheit (1973) shows that the S_1 systems cannot be produced by gas in collisional equilibrium at a single temperature. The reasons are that (*a*) Si II, Si III, and Si IV are all present in S_1 systems in comparable quantities, (*b*) C II and C IV are present also in comparable quantities, and (*c*) H I is *very* strong relative to Si and C of all species.

If the gas is then postulated to be collisionally excited at more than one temperature, the observations are found to require a minimum of two components. There must be a hot phase in which $T \sim 10^5$ K, and in which Si III, Si IV, and C IV are of comparable strength. Also, there must exist a cooler phase in which $T \sim 2 \times 10^4$ K; and in which Si II, Si III, and C II are of comparable strengths, while H I is strong and C I is very weak. We further find that the distribution of material must be strongly peaked around the two temperatures quoted. The clue to this is the Si III λ1206 line. For $4 \times 10^4\ \mathrm{K} < T < 9 \times 10^4$ K, we find that this line should be an order of magnitude stronger than the observed Si II and Si IV lines. The Si III, Si II, and Si IV lines are roughly comparable in strength; consequently, we require that only a small fraction of the material can be in the above temperature range if it is collisionally excited.

The alternative is that the gas in the S_1 systems is photoionized. From the figures of McKee, Tarter, and Weisheit (1973) we find that the line strengths are well satisfied when their parameter $\Gamma = n(\mathrm{H})/n_\gamma = 6.5 \times 10^3$. We shall henceforth discuss the physical conditions in the S_1 gas under this assumption.

First, let us consider some simple model-independent constraints that we can place on the nature of the S_1 gas clouds. The velocity dispersion in the lines is $b \lesssim 50\ \mathrm{km\ s^{-1}}$ (except when splittings occur). In some systems, there are different Doppler parameters for the low- and high-ionization species (see, e.g., $z_{\mathrm{abs}} = 2.3018$ in Q0002−422), but we do not observe a difference in the dispersions among Si and C ions at the same ionization potential (which would be in the ratio 1:1.53 if the broadening were thermal). An upper limit on the temperature, with $\sigma_v < 50\ \mathrm{km\ s^{-1}}$, is given by the carbon ions ($A = 12$); $T_{\mathrm{ions}} < Am_p\sigma_v^2/K = 4 \times 10^6$ K. The lines descend to zero intensity in both the QSO continuum light and the emission lines when the column density is sufficiently high. The implied cloud sizes are $D > 10^{16}$ cm and $D > 10^{19}$ cm, respectively (there is, of course, great uncertainty in the estimated size of the emission-line region).

Next, the typical column density of C IV and C II is $10^{15}\ \mathrm{cm^{-2}}$. Thus, $N(\mathrm{C}) \gtrsim 3 \times 10^{15}\ \mathrm{cm^{-2}}$, and the column density of hydrogen is $N(\mathrm{H}) \gtrsim 10^{19}\,(Z_\odot/Z_{\mathrm{cloud}})\ \mathrm{cm^{-2}}$, where $Z_\odot$ is the solar abundance of heavy elements and Z_{cloud} is the abundance of heavy elements for the S_1 clouds. If the cloud heavy-element abundances do not exceed solar, then this suggests that $N(\mathrm{H}) > 10^{19}\ \mathrm{cm^{-2}}$. Since we observe $N(\mathrm{H\ I}) \sim 3 \times 10^{18}\ \mathrm{cm^{-2}}$, it appears that a significant fraction of the hydrogen is neutral, as is to be expected if the S_1 gas really is in photoionization equilibrium [for the UV fluxes postulated, we expect $n(\mathrm{H\ II})/n(\mathrm{H\ I}) = 15(T/10^4\ \mathrm{K})^{1/2} n_e^{-1} \sim$ 10–100; see below].

The excited ground-state fine-structure levels Si II*($J = 3/2$) and C II*($J = 3/2$) are, as a rule, unpopulated, and, in stringent cases, we find $N(\mathrm{C\ II}^*)/N(\mathrm{C\ II}) < 0.1$, and similarly for silicon. Following the considerations of Bahcall and Wolf (1968), we find that the electron density in the gas must be $n_e \lesssim 10\ \mathrm{cm^{-3}}$. Further statements require an estimate of the photoionizing flux. If the clouds are in a galactic halo, early-type stars in the disk of the galaxy probably provide the ionizing flux. At $\lambda_c = 912$ Å, this is $J_{\nu_c}^{\mathrm{disk}} = 2 \times 10^{-20}\ \mathrm{ergs\ s^{-1}\ cm^{-2}\ Hz^{-1}\ sr^{-1}}$ within the disk of our Galaxy (de Boer, Koppenaal, and Pottasch 1973; Jura 1974); this drops to $J_{\nu_c} = J_{\nu_c}^{\mathrm{disk}}\{1 - [1 + (\mathrm{R/D})^2]^{-1/2}\} = 2 \times 10^{-21}\ \mathrm{ergs\ s^{-1}\ cm^{-2}\ Hz^{-1}\ sr^{-1}}$ at a distance $D = 20$ kpc (if the disk is a uniformly luminous slab of radius $R = 10$ kpc). Galactic starlight will not supply photons of sufficient energy to ionize C III (47.9 eV), for example. However, quasar light may well supply sufficiently energetic photons if their power-law spectra continue to follow the exponents observed in the range $\lambda > 900$ Å. In an optically thin universe, it is straightforward to compute the integrated light due to QSOs. For QSOs with luminosities $L_\nu = L_{\nu_c}(\nu/\nu_c)^{-\beta}$ ergs $\mathrm{s^{-1}\ Hz^{-1}}$ (ν_c is the Lyman limit at 912 Å), and space density $n_Q(z) = n_0 \exp\{\alpha[1 - (1 + z)^{-3/2}]\}\ \mathrm{cm^{-3}}$, we may compute the specific intensity of UV luminosity as

$$I_\nu = \frac{c}{4\pi H_0}\int_0^\infty \frac{dz n_Q(z) L_{\nu(1+z)}}{(1+z)^5(1+2q_0z)^{1/2}} = \frac{c}{4\pi H_0} n_0 L_{\nu_c}\left(\frac{\nu}{\nu_c}\right)^{-\beta}\int_0^\infty \frac{\exp\{\alpha[1-(1+z)^{-3/2}]\}(1+z)^{-\beta}dz}{(1+z)^5(1+2q_0z)^{1/2}}. \quad (10)$$

The space density of ionizing photons is then

$$\eta_\gamma = (6.32 \times 10^{-5}/\beta)(J_\nu/10^{-21})\ \mathrm{cm^{-3}}, \quad (11)$$

where $4\pi J_\nu = \int I_\nu d\varpi$. For a universe with $q_0 = 1/2$,

$$I_\nu = \frac{cn_0 L_{\nu_c}}{6\pi H_0}\left(\frac{\nu}{\nu_c}\right)^{-\beta} f(\alpha, \gamma)\,, \tag{12}$$

where $f(\alpha, \gamma) = \int_0^1 e^{\alpha(1-u)} u^\gamma du$ (this integral is a form of the incomplete Γ-function), and $\gamma = 2(\beta + 3)/3$. From the luminosity distributions of Schmidt (1970), we may estimate,

$$\sum_{\text{all QSOs}} n_0 L_{\nu_c} = 9.0 \times 10^{22} h_{100} \text{ ergs s}^{-1} \text{ Hz}^{-1} \text{ Mpc}^{-3}\,, \tag{13}$$

where $h_{100} = H_0/100$. Further, with $cH_0{}^{-1} = 9.257 \times 10^{27} h_{100}{}^{-1}$ cm and, for the $q_0 = 1/2$ universe, with $\alpha = 10.6$ [leading to $f(\alpha, \gamma) = 22$ for $\beta = 3/4$], we find

$$I_{\nu_c} = 4.0 \times 10^{-23} \text{ ergs s}^{-1} \text{ Hz}^{-1} \text{ sr}^{-1} \text{ cm}^{-2}\,, \qquad n_\gamma = 3 \times 10^{-6} \text{ cm}^{-3}\,.$$

These estimates do not change much for an $\Omega = 0$ universe because the parameters are all based on actual observed quantities. Proceeding backwards in time within the universe, at a redshift z^*, we find

$$I_\nu(z^*)/I_\nu(0) = (1 + z^*)^{-3/2}[f(\alpha^*, \gamma)/f(\alpha, \gamma)] \exp(\alpha - \alpha^*) \tag{14}$$

[where $\alpha^* = \alpha(1 + z^*)^{-3/2}$]. Thus at redshifts $z^* = 2.5$ and 1.0, respectively, we find

$$I_{\nu_c}(2.5) = 7.8 \times 10^{-22}; \qquad n_\gamma(2.5) = 3 \times 10^{-5}\,,$$

$$I_{\nu_c}(1.0) = 5.7 \times 10^{-22}; \qquad n_\gamma(1.0) = 2 \times 10^{-5}\,,$$

in the units given above. These fluxes surpass the likely contribution from galactic starlight for $\lambda < 912$ Å.

For the S_1 systems at $z_{\text{abs}} \sim 2.5$, since $n_\gamma = 3 \times 10^{-5}$ cm^{-3}, we thus find $n(\text{H}) = 0.2$ cm^{-3} for photoionization equilibrium. In order for collisional effects at these densities not to remove the C II and H I faster than they recombine, we find that the electron temperatures must satisfy $T_e \lesssim 2 \times 10^4$ K.

Calculations of the ionization conditions in the gas (including both collisions and photoionization) were made by Stephen Kent (private communication, 1978). More modern atomic data were used than in the previous calculations of McKee, Tarter, and Weisheit (1973). A power-law photoionizing flux $I_\nu = 8 \times 10^{-22}(\nu/\nu_c)^{-1}$ ergs s^{-1} Hz^{-1} sr^{-1} cm^{-2} with a density $n(\text{H}) = 0.3$ cm^{-3} reproduced the relative column densities of C II, C IV, Si II, Si III, and Si IV. For these conditions, we found $N(\text{H})/N(\text{H I}) = 30$, and we then deduce $N(\text{H}) = 10^{20}$ cm^{-2} [since $N(\text{H I}) = 3 \times 10^{18}$ cm^2]. To fit the hydrogen-to-metal column densities, we then need metal abundances depleted relative to solar abundances by a factor of 10. This conclusion is not valid if the clouds have a geometry such that portions of the gas are shielded by at least 5×10^{17} cm^{-2} of H I in every direction (an edge-on disk or end-on filament obviously violates this request), when the cloud is self-shielded by its own Lyman continuum absorption. Then the hydrogen may be mainly neutral, and we may have $N(\text{H}) < 10^{20}$ cm^{-2}. This condition will also enhance the strength of O I, N I, Mg II, and Si II lines relative to the unshielded gas, since these ions require photons just beyond the Lyman edge for their destruction.

In the ionization models, we found that the heating rate due to photoionization equaled the cooling rate at $T_e = 10^4$ K, and, with additional heat sources, we must have $T_e > 10^4$ K (if the gas is in temperature equilibrium). With the above constraints from C II and H I, we need $T_e = 1 - 2 \times 10^4$ K.

The ionization calculations and question of the metal abundances will be discussed in more detail in a later paper.

The thermalization time scales in the clouds are much shorter than the photoionization or recombination time scales. Accordingly, if the clouds are in equilibrium, they must have a size less than Jeans's length, namely $D < D_J = 1.9 \times 10^{21}(T/10^4 \text{ K})^{1/2} \sim 2.4 \times 10^{21}$ cm.

These conditions are then consistent in suggesting clouds with $D \sim N(\text{H})/n(\text{H}) \sim 3 \times 10^{20}$ cm, in accordance with the limits obtained from the line depths and Jeans's length. The mass of the hypothetical clouds is then $M \sim 10^3\, M_\odot$, this being very uncertain since it is proportional to D^2. From the galactic halo hypothesis, we require a radius of 30 kpc to be filled with these objects such that a line of sight will intersect of order one of them. This leads to $\sim 10^6$ objects per halo, and a total mass of $\sim 10^9\, M_\odot$. Thus, the halos need be only extensive, and not massive. As we have noted, the splittings at $\lesssim 150$ km s^{-1} often observed in the S_1 (and also S_2) systems correspond to the expected velocity dispersion within a galactic halo; this would provide further evidence that the halo gas is clumped.

If, on the other hand, the gas has been ejected from the particular QSO and is ionized by the QSO, we find a photon density at a distance d from the QSO of

$$n_\gamma = 9 \times 10^{-5}(1 \text{ Mpc}/d)^2(L_{\nu_c}/3 \times 10^{30}) \text{ cm}^{-3}\,,$$

and since the observations of absorption from excited fine-structure levels lead to $n_e < 10$, we find $d > 240$ kpc for photoionization equilibrium. This estimate accentuates the well-known energy problem in accelerating the gas to the velocity of $\sim 0.15c$ relative to the QSO (Goldreich and Sargent 1976). For an average of one S_1 system per QSO (or, equivalently, several, each subtending a solid angle of less than 4π), the gas mass is less than $3 \times 10^{11} M_\odot$ and the required ejection energy $\epsilon > (10^{64}/\eta)$ ergs, where η is the efficiency for the production of kinetic energy. Accordingly, we regard this alternative as implausible.

ii) *The* S_2 *Systems*

The two examples of S_2 systems in our sample of three QSOs are $z_{abs} = 0.8366$ in Q0002−422 and $z_{abs} = 0.7261$ in Q0453−423. After including the data in CSW, we find that the very strong split system $z_{abs} = 1.496/1.1516$ in Q0453−423 is also of the S_2 type, although it is formally excluded from our sample by our visibility windows.

We can be far less definitive about the nature of the S_2 systems than those of type S_1 since only the ions Mg I, Mg II, and Fe II are normally available for inspection.

The S_2 systems also imply large energies in the ejection hypothesis. For example, consider $z_{abs} = 0.7261$ in Q0453−423. The column densities of Mg I and Mg II imply $N(\text{Mg II})/N(\text{Mg I}) = 14$. The photoionizing flux at a distance d_{Mpc} from the QSO is $J_\nu = 7 \times 10^{-21} d_{\text{Mpc}}^{-2}$ ergs cm^{-2} s^{-1} Hz^{-1} sr^{-1} at 2×10^{15} Hz. The ionization equilibrium equation is

$$n_{\text{II}} n_e (\alpha_{\text{rad}} + \alpha_{\text{die}}) = n_{\text{I}} n_e \langle \sigma v \rangle + n_{\text{I}} 4\pi J_{\nu_T} a_{\nu_T} / h(\beta + \beta') , \tag{15}$$

where $J_\nu = J_{\nu_T}(\nu/\nu_T)^{-\beta}$, the photoionization cross section is $a_\nu = a_{\nu_T}(\nu/\nu_T)^{-\beta}$, the radiative plus dielectronic recombination coefficients are $(\alpha_{\text{rad}} + \alpha_{\text{die}})$, and the collision cross section is $\langle \sigma v \rangle$. For magnesium, we find

$$\begin{aligned} d_{\text{Mpc}} &= 4[n(\text{Mg I})/n_e n(\text{Mg II})]^{1/2} \left[1 + \frac{\alpha_{\text{die}}}{\alpha_{\text{rad}}} - \frac{n(\text{Mg I})}{n(\text{Mg II})} \frac{\langle \sigma v \rangle}{\alpha_{\text{rad}}} \right]^{-1/2} \\ &= 1.1 n_e^{-1/2} \left[1 + \frac{\alpha_{\text{die}}}{\alpha_{\text{rad}}} - 0.071 \frac{\langle \sigma v \rangle}{\alpha_{\text{rad}}} \right]^{-1/2} , \end{aligned} \tag{16}$$

where we have set $n(\text{Mg I})/n(\text{Mg II}) = N(\text{Mg I})/N(\text{Mg II}) = 0.071$. From Aldrovandi and Péquignot (1973), and Canto and Daltabuit (1974), we find

$$\alpha_{\text{die}}/\alpha_{\text{rad}} = 1.21 \times 10^4 T_4^{-0.645} \exp(-5.1 T_4^{-1}) , \tag{17a}$$

$$\langle \sigma v \rangle / \alpha_{\text{rad}} = 6.9 \times 10^5 T_4^{1.355} \exp(-8.88 T_4^{-1}) , \tag{17b}$$

where $T_4 = T_e/10^4$ K. The quantity in square brackets in equation (16) has a maximum at $T_4 = 1.5$ of 10^2. Thus we find

$$d_{\text{Mpc}} > 0.11 n_e^{-1/2} .$$

Since no fine-structure Fe II* is visible, we take $n_e < 10^3$ cm^{-3} (Wolfe and Wills 1977) and find $d > 4$ kpc. The cloud mass may be calculated for spherical symmetry around the QSO (since absorption-line systems are seen in all QSOs, the clouds must surround the QSOs) as $M > 3 \times 10^7 (Z_\odot/Z) M_\odot$, since $N(\text{H}) \geq N(\text{Fe II})[n(\text{H})_\odot / n(\text{Fe})_\odot](Z_\odot/Z)$, and the required energy $E > 1.3 \times 10^{61} (Z_\odot/Z)(1/\eta)$ ergs, where η is again the ejection efficiency. This limit is lower than for the S_1 systems mainly because of the less stringent limit on n_e. A similar argument, with similar numerical results, may be applied to the $z_{abs} = 0.8366$ system in Q0002−422. The conclusions may be avoided if (*a*) the Mg I and Mg II components do not arise in the same regions, or (*b*) clouds closer to the QSO shield the ionizing radiation. We note, however, that for $z_{abs} = 0.8366$ in Q0002−422, the line profiles for Mg I, Mg II, and Fe II are all similar, suggesting a common origin. In regard to ionizing radiation, Mg I requires 7.64 eV to produce Mg II, and this becomes 15.77 eV in the frame of the QSO since the clouds would be postulated to move at $0.62c$. The QSO must radiate below its Lyman edge; and absorption systems with $z_{abs} > 2.15$ are required to provide a Lyman continuum shield, with a total column density $N(\text{H I}) > 2 \times 10^{17}$ cm^{-2}. The S_1 systems cannot be invoked, since they must lie at least 200 kpc away from the QSO (see last section). In any case, one could use the system $z_{abs} = 1.1496/1.1516$ in Q0453−423 when the Mg I ionization edge is at 3487 Å. The Lyman edge of Q0453−423 is at 3336 Å, and we have low-resolution observations which show that the QSO emits radiation at least down to 3300 Å.

The other properties of S_2 systems lead to similar parameters as for the S_1 systems, viz.,

1. A typical column density $N(\text{H}) > 3 \times 10^{19} (Z_\odot/Z)$ cm^{-2} [using $N(\text{Fe}) = 10^{15}$ cm^{-2} as is observed for $N(\text{Fe II})$]. $N(\text{H})$ is increased if Fe II is not the dominant species.
2. The kinetic temperatures of the ions $T_{\text{ions}} < 5 \times 10^6$ K (from the velocity dispersions).
3. An electron density $n_e < 10^3$ cm^{-3} (from the absence of Fe II*).
4. A cloud size $D > 10^{16}$ cm (from coverage of QSO continuum light) and $D > 10^{19}$ cm (from coverage of the emission-line regions).

5. In order that collisions (apart from any photoionization) do not completely ionize Mg I [typically $N(\text{Mg II})/N(\text{Mg I}) = 100$], we must have $T \lesssim 10^4$ K.

6. If they are in equilibrium, the clouds should not exceed the Jeans's size, $D < D_J = 1.7 \times 10^{21}(T/10^4\text{ K})^{1/2}$ cm.

We can say little more than this since we do not know whether the S_2 clouds suffer significant photoionization. Because the appropriate QSO UV light is similar in strength at $z = 1$ and $z = 2.5$, the clouds would be photoionized unless they are hot and dense. It seems clear that the S_2 systems could arise from the same type of object that causes the S_1 systems; they even require the same extent of galactic halo ($\sim$30 kpc). A galactic halo, however, can undergo a great deal of evolution between $z = 1$ and $z = 2.5$, so it is by no means clear that the lines arise from similar physical situations as do the S_2 systems'.

iii) *A System with Fine Structure in* C II

Occasionally, the fine-structure state C II*($J = 3/2$) or Si II*($J = 3/2$) are seen in QSO absorption-line spectra. A convincing case is 3C 191 (Bahcall, Sargent, and Schmidt 1967), in which Si II* appears. From our sample, the only plausible fine-structure system (containing C II* but not Si II*) is $z_{\text{abs}} = 2.7685$ in PKS 2126−158. There we found $N(\text{C II*})/N(\text{C II}) = 0.3$. Let us consider this system in more detail.

From the work of Bahcall and Wolf (1968), we find that

$$n_e \leq 30\text{ cm}^{-3}$$

(applicable if $T > 10^4$ K). Equality holds if photoexcitation effects are negligible. If the gas is in photoionization equilibrium, then, as before, $n(\text{H})/n_\gamma = 6.5 \times 10^3$, and we may set a limit on the photoionizing flux: $n_\gamma \leq 4.6 \times 10^{-3}$. Because flux of this magnitude cannot photoexcite the fine-structure states (Bahcall and Wolf 1968; Bahcall 1967), we must have $n(\text{H}) = 30\text{ cm}^{-3}$ (unless the photoexcitation is by an infrared flux; it cannot be a QSO, since we must have $d \gtrsim 0.14$ Mpc from the limit on the UV flux).

This leaves us with the two possibilities:

a) The gas is in photoionization equilibrium in a UV flux $\sim 10^2$ times stronger than the intergalactic flux. It would have to be $\sim$10 times closer to a QSO than average, an event with probability $\sim 10^{-3}$.

b) The gas is in collisional equilibrium with a range of temperatures from $T = 1.5 \times 10^4$ K to $T = 10^5$ K. We note that the Si III λ1206 line is abnormally strong in this system (if it is not blended), which leads to a high column density relative to Si II and Si IV. This becomes a plausible case for collisional equilibrium with material at all temperatures between 1.5×10^4 and 10^5 K.

If the more plausible case (b) is assumed, then we may estimate the parameters of the type of cloud that can display C II*. The metal column densities suggest $N(\text{H}) \sim 10^{20}$. Since $N(\text{H I}) \approx 10^{19}$, there must be a significant amount of material with $T = 1$–2×10^4 K. However, the cloud size is $D = N(\text{H})/n_e = 10^{19}$ cm and $M \approx 100\ M_\odot$, somewhat smaller and denser than the regular S_1 clouds. The size of the cloud will enable it to totally cover a QSO continuum source and to at least partially cover the emission-line region. This is consistent with the observed line depths in PKS 2126−158 in Paper I. One system out of the three S_1 systems in our sample has shown the C II* line together with a strong Si III λ1206 line. The postulated galactic halo must then have roughly the same amount of mass ($\sim 10^9\ M_\odot$) in these slightly smaller and denser clouds.

The problem with these clouds is, first, the large pressure required to confine the gas at $T = 10^4$ K and $n_e = 30$ cm^{-3} (if the clouds are actually in equilibrium and not expanding, for example), and, second, the high density that implies a cooling rate much greater than the photoionization heating rate (from QSO light). Auxiliary heating sources or rapid cooling (and lack of equilibrium) must be postulated.

IV. CONCLUSIONS

We have presented new, high-resolution data for two QSOs, computed data on the emission and absorption systems, and identified five absorption-line systems of differing probability in each QSO. These data were then added to that contained in Paper I (on PKS 2126−158) for an analysis of the properties of the identified absorption systems in high-redshift QSOs.

From an examination of these heavy-element absorption systems in the three high-redshift QSOs, we find the following:

1. The systems are similar in type, line strength, velocity dispersion, and redshift distribution among the QSOs.
2. If supposed to arise in galactic halos, a radius of 30 kpc of absorbing material is required. If postulated to come from disks, the radius must be increased by $2^{1/2}$.
3. If ejected from the QSO, energies of $(10^{64}/\eta)$ ergs are required, where η is the ejection efficiency.
4. The systems (S_1) at high redshift, $z_{\text{abs}} \sim 2.5$, are probably in photoionization equilibrium. The clouds responsible for the absorption probably have parameters close to the following:

$$n(\text{H}) = 0.3\text{ cm}^{-3}, \quad T_e = 10^4\text{ K}, \quad N(\text{H}) = 10^{20}\text{ cm}^{-2}; \quad D = 3 \times 10^{20}\text{ cm},$$
$$M = 10^3\ M_\odot, \quad n(\text{H})/n(\text{H I}) = 30.$$

They cannot supply a cosmologically interesting mass density, with $\Omega_{\rm cloud} = 10^{-3}$ for the S_1 and W_1 type systems.

5. The systems (S_2) at low redshift, $z_{\rm abs} \sim 1$, must satisfy

$$N({\rm H}) > 3 \times 10^{19}\ {\rm cm}^{-2}, \quad T_e < 10^4\ {\rm K}, \quad 10^{19}\ {\rm cm} < D < 2 \times 10^{21}\ {\rm cm},$$

$$n_e < 10^3\ {\rm cm}^{-3}, \quad n({\rm H}) > 10^{-2}\ {\rm cm}^{-3}.$$

In principle, they can be the same type of object that produces the S_1 systems, although, of course, this is not necessarily the case. The S_2 and W_2 type systems together contribute a cosmological density $\Omega_{\rm cloud} \sim 10^{-3} \times [N({\rm H})/10^{20}\ {\rm cm}^{-2}]$.

6. If the clouds are in galactic halos, then $\sim 10^6$ clouds per halo are required, with a total mass of $\sim 10^9\ M_\odot$. They may arise from the disks of galaxies, but the splittings strongly suggest that at least some must arise from halo clouds (the probability that the line of sight intersects two different galaxy disks in the same group [e.g., the Local Group] would be $\sim 3 \times 10^{-3}$ times the probability of intersecting one).

We conclude that the evidence presented here must support the "intervening galaxy" hypothesis rather than the ejection hypothesis for the origin of the QSO absorption lines. This conclusion applies to all the heavy-element systems, at both high and low redshifts. The reasons are that by careful study with well-defined samples we have (*a*) alleviated the requirement for large galactic halos; we only need halos about 30 kpc in extent for galaxies with $M_{B(0)} = -19$ to produce S_1 and S_2 systems, and 50 kpc radius for W_1 and W_2 systems; (*b*) exacerbated severely the well-known ejection-energy problem; and (*c*) shown, from a preliminary sample, that the redshift systems in different QSOs are similar in all respects, as is predicted by the intervening hypothesis.

We thank the UK Panel for Allocation of Telescope Time for the generous allotment of time which made the observations possible, and for financial support. The development of the IPCS was financed with the aid of grants from the UK Science Research Council. W. S. thanks the National Science Foundation for a travel grant. Other work by W. S. and P. J. Y. was supported by National Science Foundation grant ATS 75-00555. We thank Stephen Kent for performing various computations and for many valuable discussions.

REFERENCES

Aaronson, M., McKee, C. F., and Weisheit, J. C. 1975, *Ap. J.*, **198**, 13.
Aldrovandi, S. M. V., and Péquignot, D. 1973, *Astr. Ap.*, **25**, 137.
Bahcall, J. N. 1967, *Ap. J. (Letters)*, **149**, L7.
———. 1975, *Ap. J. (Letters)*, **200**, L1.
Bahcall, J. N., Sargent, W. L. W., and Schmidt, M. 1967, *Ap. J. (Letters)*, **149**, L11.
Bahcall, J. N., and Wolf, R. A. 1968, *Ap. J.*, **152**, 701.
Boksenberg, A., Carswell, R. F., and Sargent, W. L. W. 1979, preprint.
Boroson, T., Sargent, W. L. W., Boksenberg, A., and Carswell, R. F. 1978, *Ap. J.*, **220**, 772.
Burbidge, G., O'Dell, S. L., Roberts, D. H., and Smith, H. E. 1977, *Ap. J.*, **218**, 33.
Canto, J., and Daltabuit, E. 1974, *Rev. Mexicana Astr. Ap.*, **1**, 5.
Carswell, R. F., Smith, M. G., and Whelan, J. A. J. 1977, *Ap. J.*, **216**, 351 (CSW).
de Boer, K. S., Koppenaal, K., and Pottasch, S. R. 1973, *Astr. Ap.*, **28**, 145.
Goldreich, P., and Sargent, W. L. W. 1976, *Comm. Astr. Ap.*, **6**, 133.
Holmberg, E. 1976, in *Galaxies and the Universe*, ed. A. Sandage, M. Sandage, and J. Kristian (Chicago: University of Chicago Press), p. 123.
Jura, M. 1974, *Ap. J.*, **191**, 375.
Lynds, C. R. 1971, *Ap. J. (Letters)*, **164**, L73.
McKee, C. F., Tarter, B. C., and Weisheit, J. C. 1973, *Ap. Letters*, **13**, 13.
Morton, D. C. 1975, *Ap. J.*, **197**, 85.
———. 1978, *Ap. J.*, **222**, 863.
Morton, D. C., and Smith, W. H. 1973, *Ap. J. Suppl.*, **26**, 333.
Osmer, P. S., and Smith, M. G. 1976, *Ap. J.*, **210**, 267.
Sargent, W. L. W., Young, P. J, Boksenberg, A., Shortridge, K., Lynds, C. R., and Hartwick, F. D. A. 1978, *Ap. J.*, **221**, 731.
Schecter, P. 1976, *Ap. J.*, **203**, 297.
Schmidt, M. 1970, *Ap. J.*, **162**, 371.
Smith, M. G. 1975, *Ap. J.*, **202**, 591.
———. 1976, *Ap. J. (Letters)*, **206**, L125.
Whelan, J. A. J., Carswell, R. F., and Smith, M. G. 1977, *M.N.R.A.S.*, **181**, 81P (WCS).
Wolfe, A. M., and Wills, B. J. 1977, *Ap. J.*, **218**, 39.
Young, P. J, Sargent, W. L. W., Boksenberg, A., Carswell, R. F., and Whelan, J. A. J. 1979, *Ap. J.*, **229**, 891. (Paper I).

Note added in proof.—In Tables 3 and 5, line 12 (λ3940.3), the observed equivalent width should be 2.1 Å. In Table 4, line 34 (λ4233.0), the observed equivalent width should be 2.3 Å.

A. Boksenberg: Department of Physics and Astronomy, University College London, Gower Street, London WC1E 6BT, England

R. F. Carswell and J. A. J. Whelan: Institute of Astronomy, Cambridge University, Madingley Road, Cambridge CB3 0HA, England

Wallace L. W. Sargent and Peter J Young: Department of Astronomy 105–24, California Institute of Technology, Pasadena, CA 91125